2007

Comparative study on Double-Rotor PM brushless motors with cylindrical and disc type slot-less stator

Pavani Gottipati

Louisiana State University and Agricultural and Mechanical College, pavani.gottipati@gmail.com

Recommended Citation

COMPARATIVE STUDY ON DOUBLE-ROTOR PM BRUSHLESS MOTORS
WITH
CYLINDRICAL AND DISC TYPE SLOT-LESS STATOR

A Thesis
Submitted to the Graduate Faculty of the
Louisiana State University and
Agricultural and Mechanical College
in partial fulfillment of the
requirements for the degree of
Master of Science in Electrical Engineering

in

The Department of Electrical & Computer Engineering

by
Pavani Gottipati
Bachelor of Technology, Andhra University, 2004
August 2007

Dedicated to my dearest parents

ACKNOWLEDGEMENTS

TABLE OF CONTENTS

LIST OF TABLES

LIST OF FIGURES

ABSTRACT

Among brushless permanent magnet machines, the torus motors (also called Axial Flux Double-Rotor Permanent Magnet (AFTR PM) motors) are most compact and highly efficient. A cylindrical counterpart of this motor is a newly proposed Radial Flux Double-Rotor Permanent Magnet (RFTR PM) motor.

The objectives of this thesis are to optimize the magnetic circuit of both AFTR PM and RFTR PM motors and to compare their electromechanical parameters on the basis of the results obtained from magnetic field simulation using Finite Element Method (FEM).

To reach these objectives, FEM models are developed for both the motors, for particular given data. Applying the magnetic field simulation with the help of FEMM 4.0 software package, optimized stator and rotor core dimensions were determined as well as electromechanical parameters such as electromechanical torque, electromotive force, resistance and inductance of the stator windings. Next, the efficiency and torque to volume ratio along with the torque to mass ratio were calculated.

Comparing the parameters of both motors, the following conclusions are obtained:

- Both slot-less motors developed electromagnetic torque with very low torque ripple contents.

- The torque to mass ratio of RFTR PM motor is almost equal to the torque per mass of AFTR PM machine.

- AFTR PM motor is more compact than its cylindrical counterpart because its torque to volume ratio is higher.

- The efficiency of RFTR PM motor is relatively higher than that of AFTR PM motor, particularly if multi disc motor is considered, mainly due to the smaller percentage of end connection in the entire volume of the winding.

CHAPTER 1: INTRODUCTION

1.1 Overview of the Thesis

The Brushless Permanent Magnet Motors (BPMMs) are more and more applied in different types of electric drives. They are characterized by high efficiency and high value of developed electromagnetic torque to motor mass ratio [1].

If motor geometry is considered, cylindrical shape motors are most often met. Among motors with a flat geometry, disc motors are applied where the longitudinal dimensions of the mechanical device is limited. The wheel chair or an electric car may be considered as an example, where motor is embedded in the wheel rim (see Figure 1.1). Another example is an elevator where the drive is placed aside the moving cabins (see Figure 1.2).
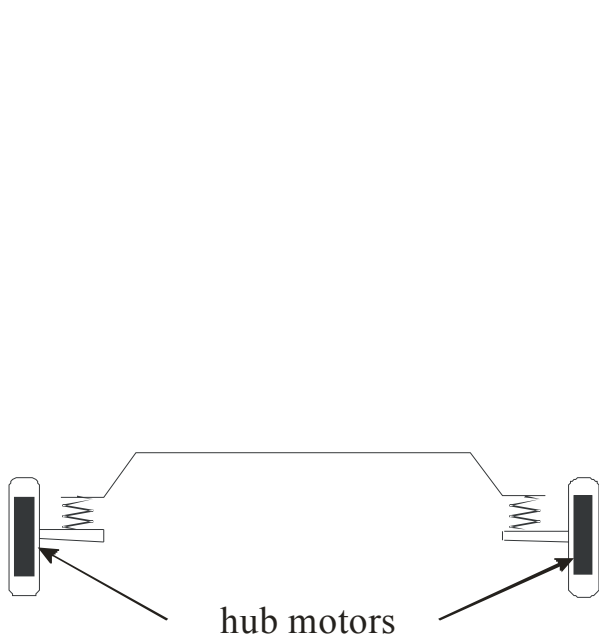
Fig.1.1 (a): Car driven by two in-wheel-motors
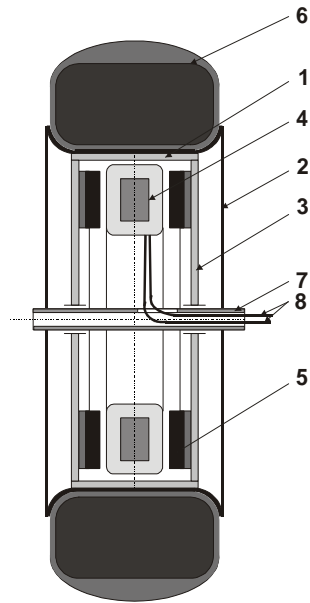
Fig.1.1 (b) Wheel with Hub motor: 1 – torus motor, 2 – wheel rim, 3 – rotor, 4 - stator, 5 – permanent magnet, 6 – tire, 7 – wheel axel, 8 – supply wires

Figure 1.1: In-wheel-motor of an electric car
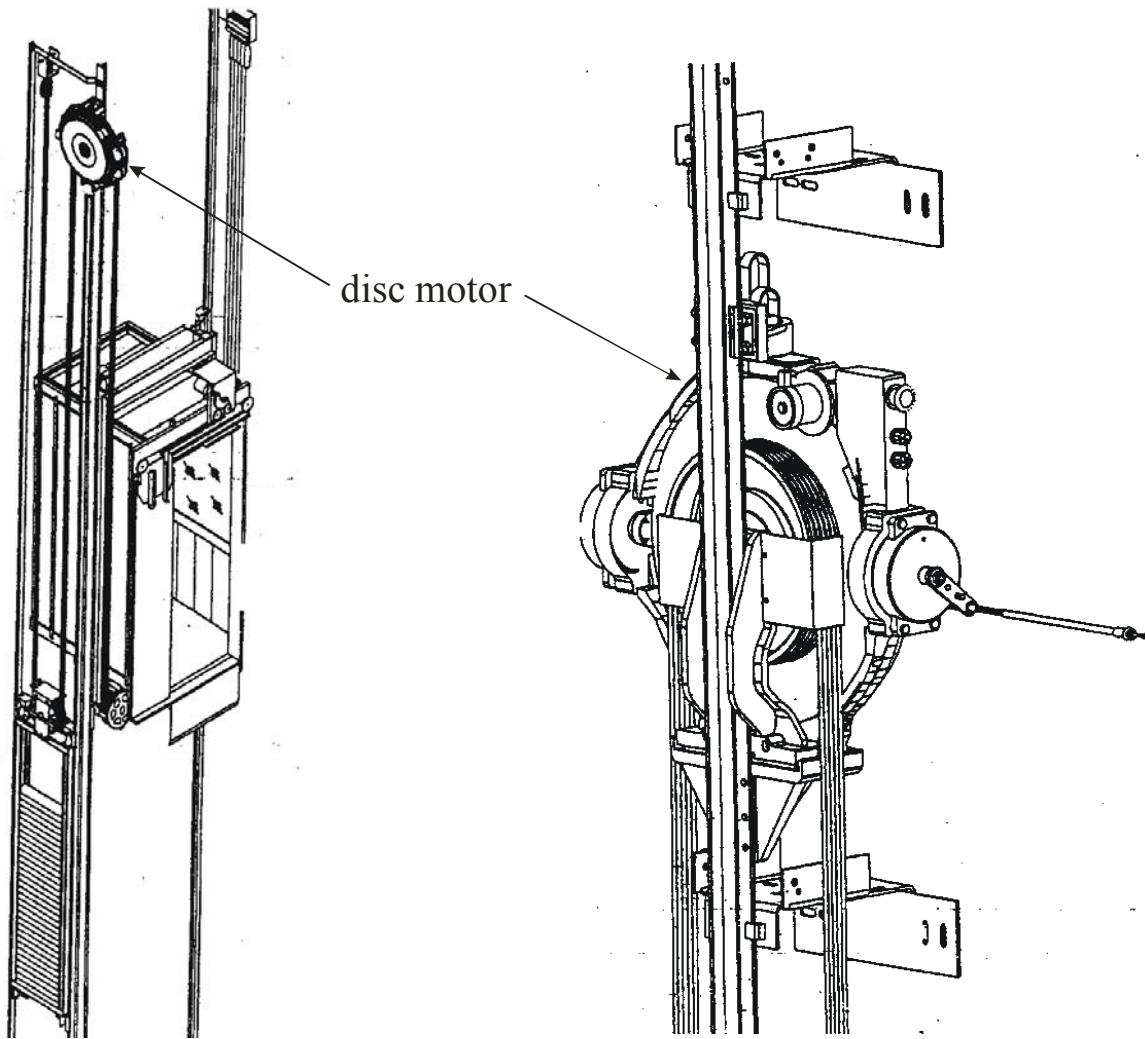
Figure 1.2: Elevator with the drive placed aside the cabin [2]

Among the disc type motors, the most compact structure has the motor with twin rotor and Gramme's type winding. These motors built in the version with slotless stator are called torus motors. They develop a relatively constant electromagnetic torque with the negligible contents of higher harmonics. These motors with "noiseless" operation are used in the mechanisms where the torque ripple cannot be tolerated, e.g. wheelchairs and elevators.

A counterpart of torus motor, but with cylindrical structure is twin rotor BPMM. Both torus motor and twin rotor cylindrical motor are the objects of the study.

1.2 Objectives of the Thesis

The objectives of this thesis are:

- To optimize the dimensions of disc-type and cylindrical motors with slot-less stator.

- To determine and compare the electromechanical parameters of both the motors mentioned above.

The tasks to be accomplished are as follows:

- A literature study on:

    o Double-rotor PM brushless motors

    o Finite Element Method

- Developing a 2-D model of the disc-type and cylindrical shape PM brushless motors using the software package FEMM 4.0

- Determining the motor core dimensions and the electromechanical parameters of both the motors using the FEMM models

- Comparison of the simulation results obtained from FEMM to evaluate the performance of the motors

1.3 Outline of the Thesis

- Chapter 2 provides an introduction to the PM brushless motors, its principle of operation and the design types. The disc-type and the cylindrical shape double-rotor PM brushless motors are briefly discussed.

- Chapter 3 discusses the Finite Element Method used to solve the Maxwell equations. Information about creating the models and analyzing the results is also included in this chapter.

- Chapter 4 presents the FEMM model for disc-type double-rotor PM brushless motor, based on the design data provided. The motor core dimensions and electromechanical parameters are then determined.

- Chapter 5 provides the simulation model for cylindrical shape double-rotor PM brushless motor in FEMM. Also, the dimensions of rotor and stator; and the torque distribution curves are obtained from the model.

- Chapter 6 compares the parameters obtained for disc-type and cylindrical shape PM brushless motors and presents a conclusion to this thesis and points to the direction of future research.

CHAPTER 2: DOUBLE-ROTOR PM BRUSHLESS MOTORS

The motor feature that distinguishes the Permanent Magnet Motors (PMM) from any other machines is the excitation. The PMMs are excited by permanent magnets, while all other machines by excitation winding.

2.1 PM Brushless Motors: Principle of Operation and Design Types

Among PMMs, if the type of winding supply is considered, two groups of machines may be specified:

- Commutator PMMs (with brushes)

- Brushless PMMs (no commutator)

The commutator PMMs are DC commutator motors. The commutator is the part of these machines, which essentially differs them from brushless PMMs. Another feature that differs them from all brushless PMMs is that the permanent magnets are placed on the stator. In brushless PMMs, these PMMs are mounted on the rotor. Figure 2.1 shows the differences and similarities which characterize these two machines.
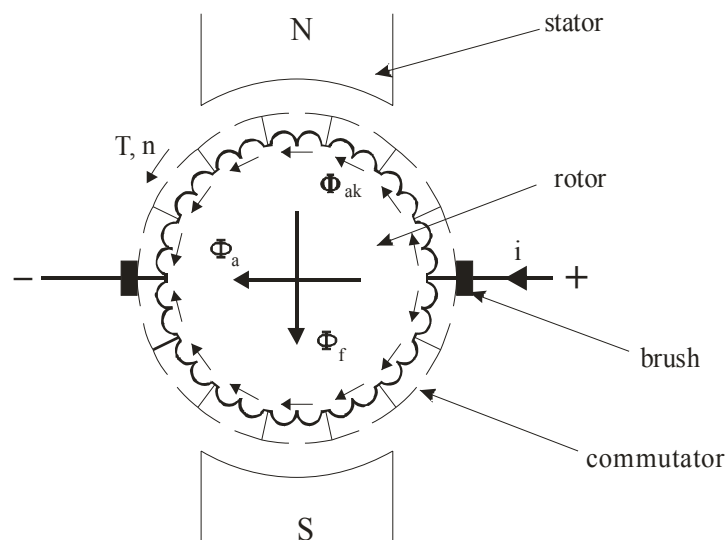
Figure 2.1 (a): Schematic of a DC commutator motor
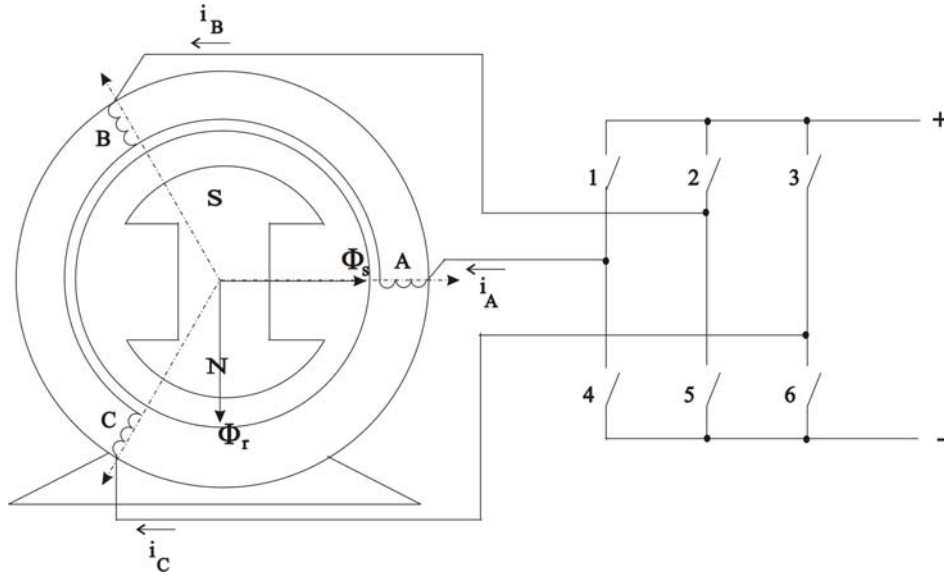
Figure 2.1(b): Schematic of a brushless permanent magnet motor

Figure 2.1 (a) shows the scheme of commutator PMM. The rotor winding, simplified to three coils connected in series, is supplied from a DC source through the commutator and brushes. The resultant flux, Φ_a obtained as a sum of three coil fluxes is perpendicular to the axis of the PM flux axis. Despite the rotor rotation, it does not change its position due to the commutator. The interaction of the two magnetic fluxes gives electromagnetic torque, T_{em} which may be expressed as follows:

$$T_{em} = K_T \times \Phi_f \times \Phi_a \tag{2.1}$$

where $\qquad$ K_T is the proportionality constant

$\qquad$ Φ_f is the excitation flux of PMs

$\qquad$ Φ_a is the armature (rotor) magnetic flux

The two fluxes Φ_a and Φ_f are stationary.

In brushless DC PMM, the rotor flux rotates. Thus the flux of the stator should rotate too with the same speed. To do this, the three phases of the stator should be supplied alternatively as shown in Figures 2.2 and 2.3. Figure 2.2 (b) shows the transistors 1 and 6 closed, thus phases A

and C are supplied. After $\omega t = 60^{\circ}$, the phases A and B are supplied as shown in Figure 2.3 (b) and the two magnetic fluxes Φ_a and Φ_f changed their position by angle $\theta = 60^{\circ}$. Figures 2.2 (a) and 2.3 (a) show how the rotor winding of commutator PM motor is supplied through the commutator, at two different rotor positions adequate to the change of rotor position of brushless DC PM motors.

(a)

(b)
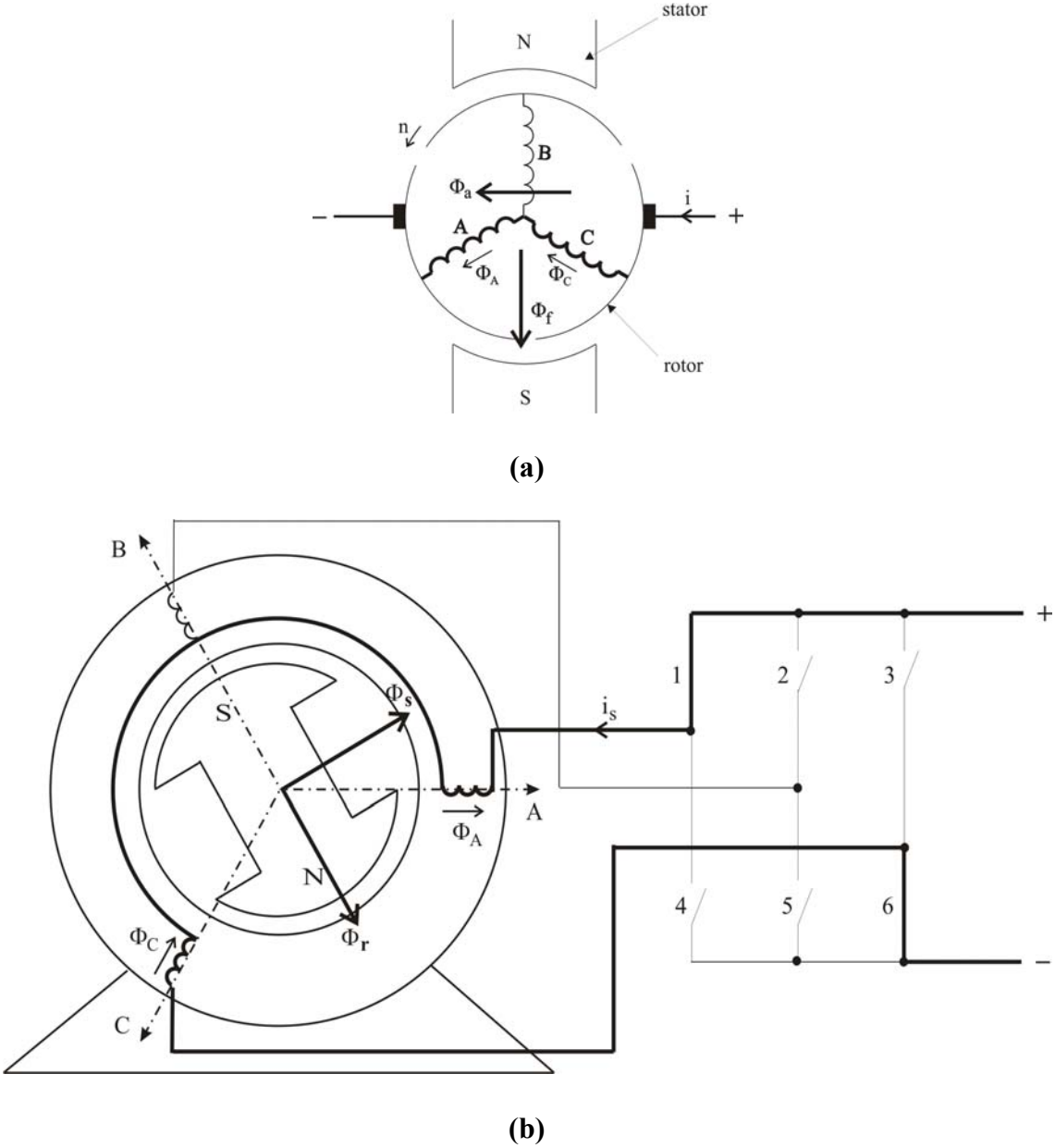
Figure 2.2: Position of the rotor and stator fluxes at time instant t_1: (a) commutator PM motor, (b) brushless DC PM motor
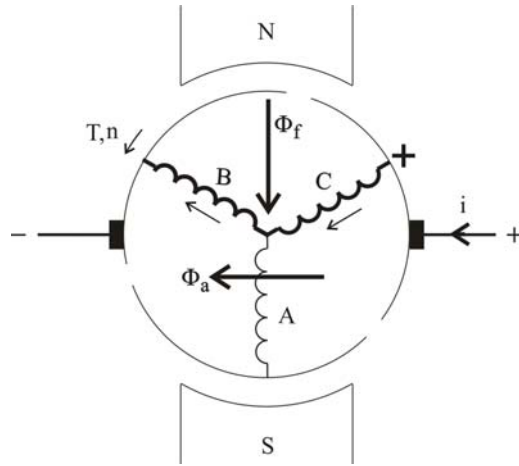
(a)
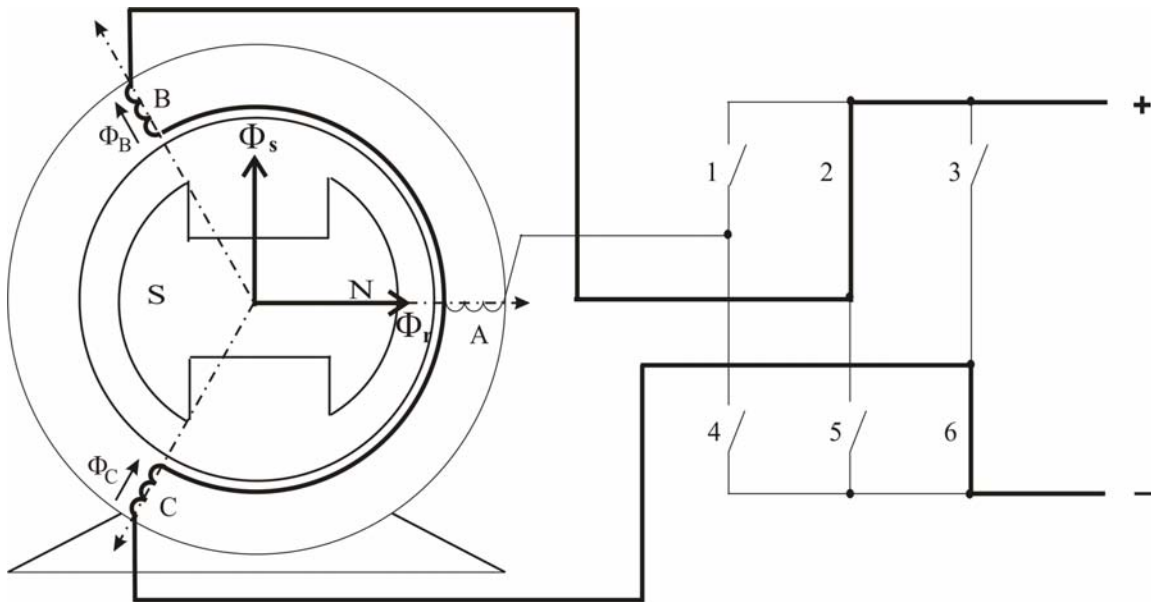
(b)

Figure 2.3: Position of the rotor and stator fluxes at time instant t_2 ($\omega t_2 = \omega t_1 + 60^\circ$): (a) commutator PM motor, (b) brushless PM motor

The advantages and disadvantages of a conventional DC motor and a brushless DC motor are discussed in Table 2.1.

Table 2.1: Comparison of conventional and brushless DC motors [3]

	Conventional motors	Brushless motors
Mechanical structure	Field magnets on the stator	Field magnets on the rotor
Winding connections	Ring connection The simplest: Δ connection	Δ or Y-connected three-phase winding or a two-phase connection
Commutation method	Mechanical contact between brushes and commutator	Electronic switching using transistors
Detecting method of rotor's position	Automatically detected by brushes	Hall element, optical encoder, etc
Reversing method	By reversal of terminal voltage	Rearranging logic sequencer
Distinctive features	Quick response and excellent controllability	Long-lasting and easy maintenance

To supply the appropriate phase of the brushless PMM, a position sensor should be applied. A signal from this sensor gives information to the controller about which phases should be supplied. The controller then switches these phases. It means the brushless DC PM motor operates with the position feedback loop as shown in Figure 2.4 (a). The frequency the three phases are supplied depends on the speed of the rotor.
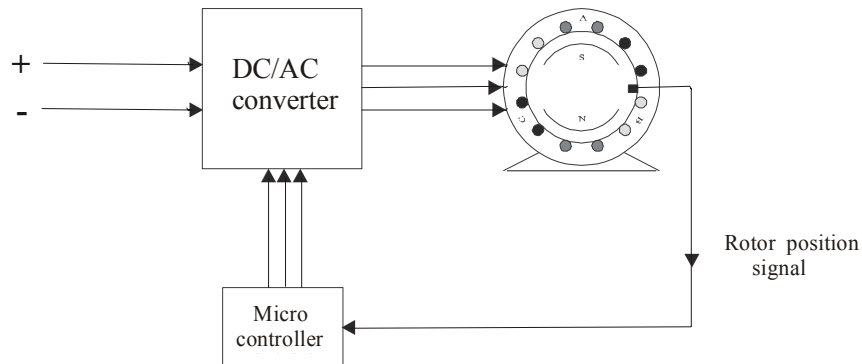
Figure 2.4 (a): Supply circuit scheme of the brushless DC PM motor [1]

The brushless PM motor can operate without position feedback loop as shown in Figure 2.4 (b). In this case, the controller switches the three phase winding with the reference frequency. This type of operation of brushless PM motor is similar to the operation of synchronous machine. The rotor is forced to rotate synchronously with the stator magnetic flux, whose speed ω_1 is related to the supply frequency f, according to the equation

$$\omega_1 = \frac{2\pi f}{p/2} \tag{2.2}$$

where p is the number of poles.
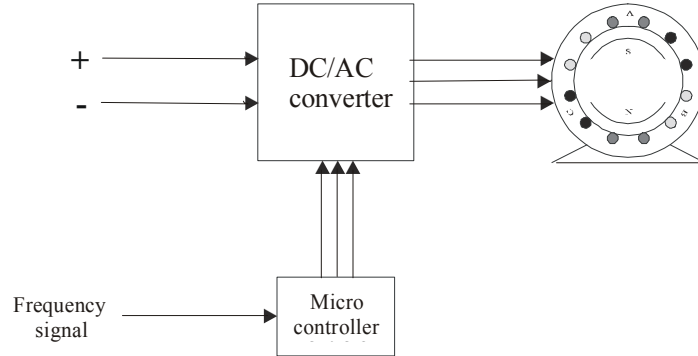
Figure 2.4 (b): Supply circuit scheme of the synchronous permanent magnet motor

From above reasoning, it is seen that brushless DC PM motor does not differ in construction from brushless synchronous PM motor. The difference between these two motors lies in the control of supply circuit. This influences the motor performance of these two motors. One of the major difference in their operation is that brushless DC PM motor operates with the speed that varies with the load, while the speed of brushless synchronous PM motor is constant at the variable load. Another difference is that the brushless DC PM motor develops the starting torque while the synchronous motor does not.

A PM DC motor is basically the same machine as a shunt or separately excited dc motor, except that the flux of a PMDC motor is fixed. Therefore, it is not possible to control the speed

of a PMDC motor by varying the field current or flux. The only methods of speed control available for a PMDC motor are armature voltage control and armature resistance control.

The use of permanent magnets in construction of electrical machines brings the following advantages over the electromagnets:

- Since these motors do not require an external field circuit, they do not have the field circuit copper losses (the excitation losses) and thus the efficiency of these motors is significantly higher than that of the wound-field motors.

- Because no field windings are required, they can be smaller than corresponding shunt dc motors, also resulting in simplification of construction and maintenance.

- Higher torque and/or output power per volume and better dynamic performance than motors using electromagnetic excitation [4].

- In very small ratings, use of permanent magnet excitation results in lower manufacturing cost.

- Low voltage PMDC motors produce less air noise and also little radio and TV interference.

A good material for the poles of a PMDC motor should have as large a residual flux density B_r as possible, while simultaneously having as large a coercive magnetizing intensity H_c as possible, see Figure 2.5.

There are basically three different types of permanent magnets which are used in DC motors:

 i. Alnico magnet – very high flux density but low coercive force

ii. Ferrite or ceramic magnet – low flux density but high coercive force

iii. Rare-earth magnet (samarium-cobalt and neodymium-iron-cobalt magnets) – both high magnetic remanence and high coercive force

The third type of magnets are used in brushless PM motors. The parameters of these magnets are shown in Table 2.2.
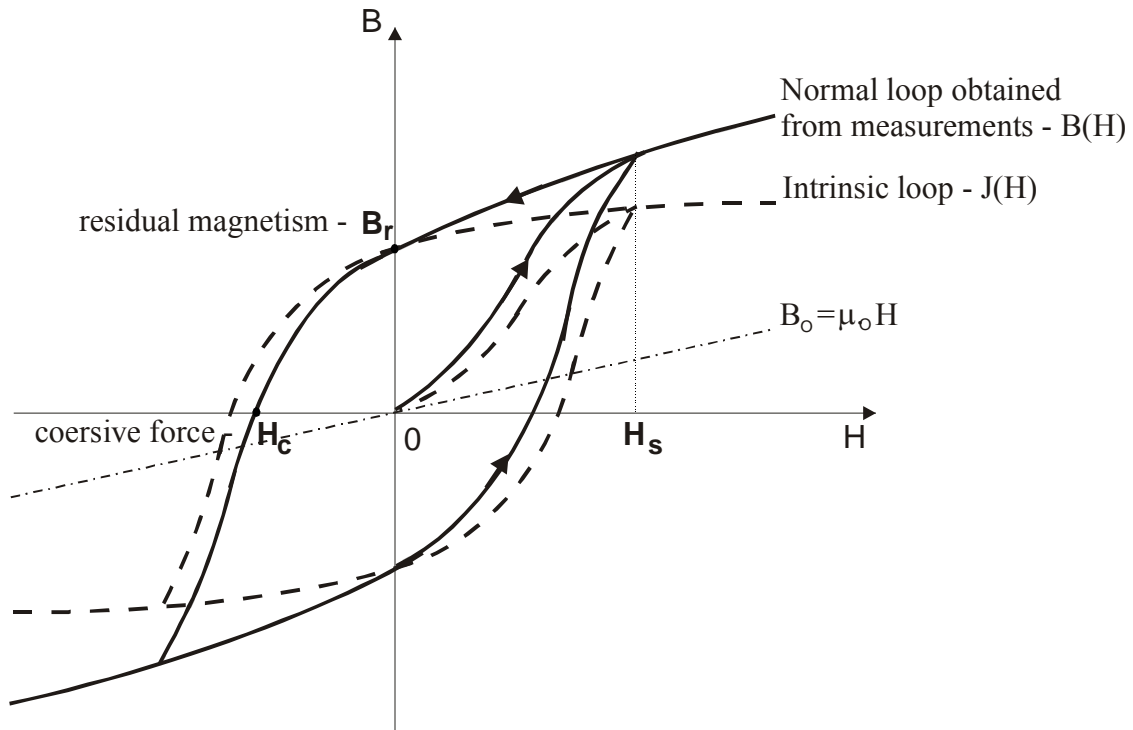
Figure 2.5: The magnetization curve of a typical ferromagnetic material [1]

Table 2.2: Parameters of permanent magnet materials [1]

	$(B \cdot H)_{max}$ [kJ/m^3]	B_r [T]	H_c [kA/m.]
Ceramics	27 – 35	0.4	240
Alnico	70 - 85	1.1	130
Rare earth magnets:			
- SmCo$_5$	160 – 200	0.9 – 1.0	660 – 750
- Sm$_2$Co$_{17}$	205 - 240	1.04 – 1.12	760 – 820
- Nd-Fe-B	190 - 385	1.0 – 1.4	760 – 980

PMDC motors with ceramics or Alnico magnets also have disadvantages:

- Permanent magnets cannot produce a flux density as high as an externally supplied shunt field, so PMDC motor will have a lower produced torque per ampere of armature current than a shunt motor of the same size and construction.

- A more serious disadvantage is that the permanent magnets can be demagnetized by armature reaction mmf causing the motor to be inoperative.

These disadvantages do not concern the motors with rare earth magnets.

The armature current in a DC machine produces an armature magnetic field of its own. The armature mmf subtracts from the mmf of the poles under some portions of the pole faces and adds to the mmf of the poles under other portions of the pole faces, reducing the overall net flux in the machine. This is the armature reaction effect. Demagnetization can result from: *(a)* improper design, *(b)* excessive armature current caused by a fault or transient or improper connection in the armature circuit, *(c)* improper brush shift and *(d)* temperature effects, like excessive heating which can occur during prolonged periods of overload [5].

- Another disadvantage with the conventional PMDC motor is the requirement of maintenance caused by the mechanical wear out of brushes and commutator.

The advantage of synchronous and DC brushless motors over DC commutator motors is that the armature current of the former is not transmitted through brushes, thus reducing the wear and need for maintenance. Another advantage of brushless motor is the fact that the power losses occur in the stator, where heat transfer conditions are good. Consequently the power density can be increased as compared with a DC commutator motor. In addition, considerable improvements in dynamics of brushless PM motor drives can be achieved since the rotor has a lower inertia and

there is a high air gap magnetic flux density and no-speed dependent current limitation. Thus, the volume of a brushless PM motor can be reduced by more than 40% while still keeping the same rating as that of a PM commutator motor.

2.2 Disc-Type Double-Rotor PM Motor

Among several types of disc type permanent magnet DC brushless motors, two constructions have been most frequently proposed:

- Motor with axial flux in the stator

- Torus type motor

Axial flux PM (AFPM) motors can be designed as double-sided or single sided machines, with or without armature slots, with internal or external PM rotors and with surface mounted or interior type PM's [4]. A common type of AFPM motor is torus type motor. A disc-type brushless dc motor with double sided stator and twin rotors, is called a torus motor. Figure 2.6 shows a schematic of the torus motor.
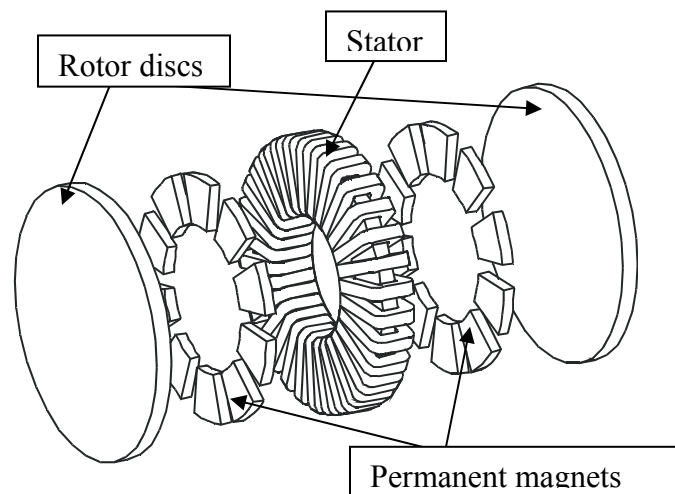
Figure 2.6: Scheme of a torus motor [6]

In a torus motor, the stator core is positioned between two rotors and each rotor disc carries axially-magnetized permanent magnets which are mounted radially on the surface turned

14

to stator structure. The stator consists of a slot-less core, made of laminated iron and the Gramme's type winding. The rotor disc is made of solid iron. As a result of this arrangement, the permanent magnets on the rotor disc force the flux to pass through air-gaps into the stator; the flux then travels circumferentially along the stator core, back across the air-gap and PM, and then back through the back iron. The distribution of magnetic flux in the disc shape torus motor is shown in Figure 2.7.
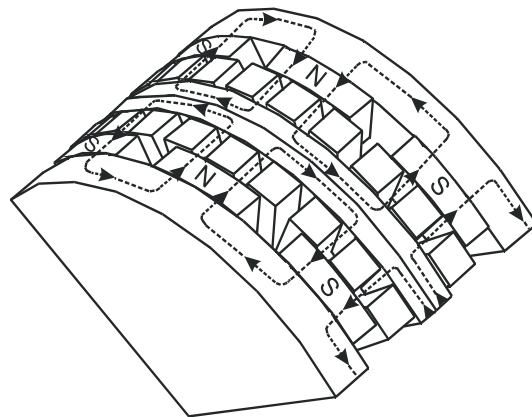
Figure 2.7: Magnetic flux distribution in a disc shape torus motor

The stator is equipped with Gramme's type winding consisting of coils wound on the toroidal stator core. Having this type of winding, the two working surfaces of core are used. This results in a higher percentage of the stator winding that produce torque compared with conventional machines having winding placed in slots. The current flowing through each coil interacts with the flux generated by magnets producing a force tangential to the machine axis. Figure 2.8 shows a working prototype of a slotless stator double-rotor disc shape torus motor.

Furthermore, the two rotating discs act naturally as fans, so that the rotor structure can be suitably designed in order to remove the machine heating due to copper and iron stator losses. The task related to heat removal can be achieved by means of holes positioned near the

mechanical shaft, so that a flow of air is sustained radially through the machine air-gap and cooling is provided thereby.
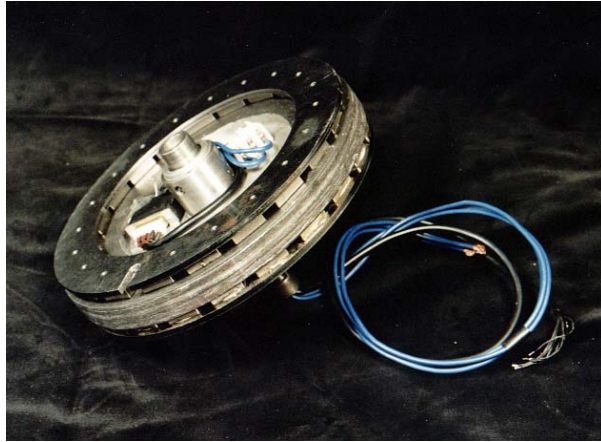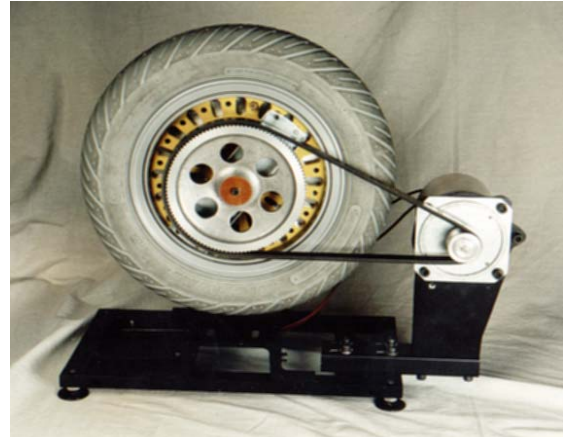
<div align="center">(a)   (b)</div>

Figure 2.8: Prototype of the slotless stator double-rotor disc shape torus motor: (a) two disc rotors and stator between, (b) wheel with torus motor [17]

The features of the motors with disc rotors are small axial dimensions and, at larger rotor diameters, these motors have better parameters than in the motors with cylindrical rotors. Moreover, the disc motors can be designed in such a way that mechanical speed reducers become unnecessary. High-energy permanent magnets enable obtaining of high magnetic flux density in machine working air gaps in the presence of simultaneously low values of permeability. Flat structure of disc rotors is more advantageous technologically and favors an application of elements made of hard magnetic materials in the form of plate.

To increase the torque developed by the motor, multi-layer disc motor can be used (Figure 2.9). Multi-layer disc motors have better magnetic field distribution and minimal leakage magnetic flux than cylindrical ones [7]. Thus, the multi-layer disc motor has increased torque and output mechanical power. Besides, the control windings of the multi-layer disc motor have

much better thermal conditions, and, for the same torque and size, the efficiency of this motor is much higher, since the current density can be three or four times lower.
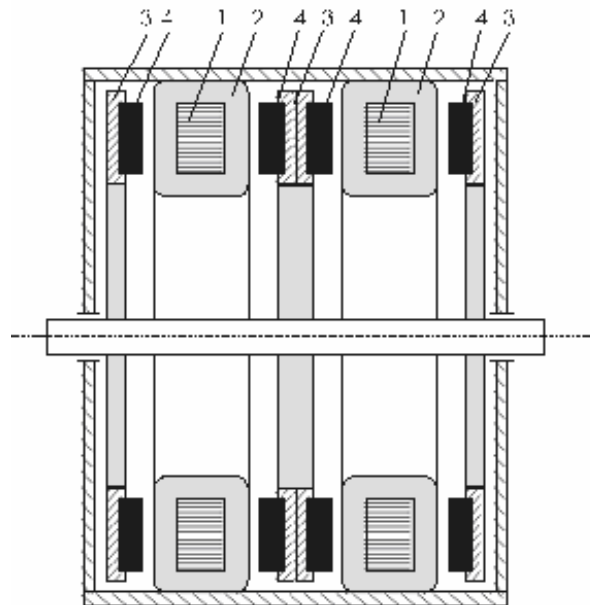
Figure 2.9: Multi-layer disc motor: 1-stator core, 2-stator winding, 3-rotor, 4-magnets [6]

However, the reasons for shelving the axial flux machine may be summarized as follows:

- Strong axial (normal) magnetic attraction force between the stator and rotor

- Difficulties in assembling the machine and keeping the uniform air gap between the stator and rotor

- Fabrication difficulties, such as cutting slots in laminated cores and other methods of making slotted stator cores

- High costs involved in manufacturing the laminated stator cores

2.3 Cylindrical Shape Double-Rotor PM Motor

The cylindrical motors which are commonly used have one stator and one rotor. The stator winding usually embraces the rotor which is an inner part of the motor. Sometimes the rotor is an outer part of the motor. This type of motor is applied in gearless drives. Figure 2.10

shows the scheme of the cylindrical motor embedded in the wheel rim used in gearless drive of electric vehicles.
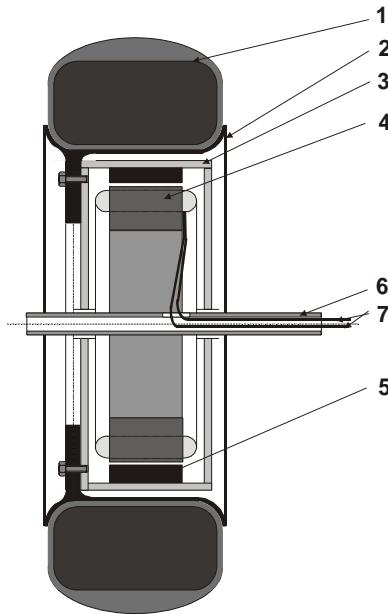
Figure 2.10: Cylindrical PM motor attached to the wheel rim: 1 - tire, 2 - wheel rim, 3 - rotor, 4 - stator, 5 - permanent magnets, 6 - wheel axle, 7 - supply wires

Referring to torus motors which have the Gramme's type winding with short end connections, the conventional cylindrical motors have the winding with much longer end connections. This, of course, contributes to much bigger use of copper wire and an increase of winding losses. To reduce these deficiencies, a cylindrical motor with two sided stator and twin rotor has been proposed by the supervisor of this MS thesis.

The cylindrical motor with twin rotor (CMTR) is a modified version of the torus motor (see Figure 2.11). The cylindrical version may be obtained in the way in which the torus motor is extended in axial direction and shortened in radial direction and the side rotors are moved to radial location.

This CMTR has also Gramme's type winding with short end connections which ensure the small winding losses. Among the elements that differ this motor from AFTR PM motor is the

type of lamination of stator core. Since the magnetic flux of both rotors is crossing the air gap in radial direction and then is passing through the stator core in circumferential direction (see Figure 2.11), the stator core has to have the lamination in axial direction as all conventional cylindrical motors.
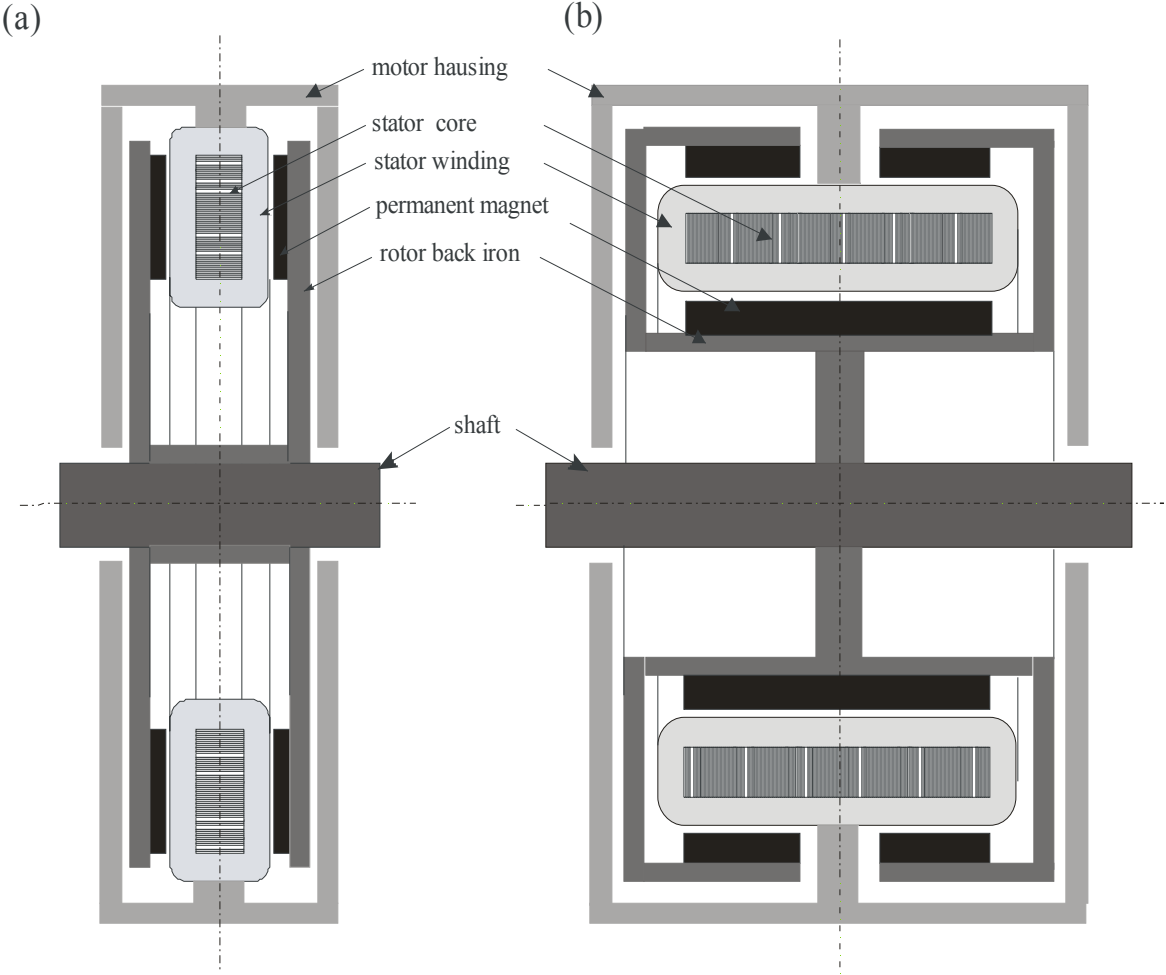
Figure 2.11: Cylindrical motor as a modified version of torus motor

The structure of RFTR PMM considered in this project is shown in Fig 2.12. The motor has inner and outer part of the rotor connected firmly together by the side disc. The permanent magnets are attached to the rotor cylindrical surfaces adjacent to the stator coils. The stator slot-less core is attached to the motor housing.

A

motor housing
solid iron rotor cylinder
permanent magnet
laminated stator core
stator winding
permanent magnet
solid iron rotor cylinder

shaft

A
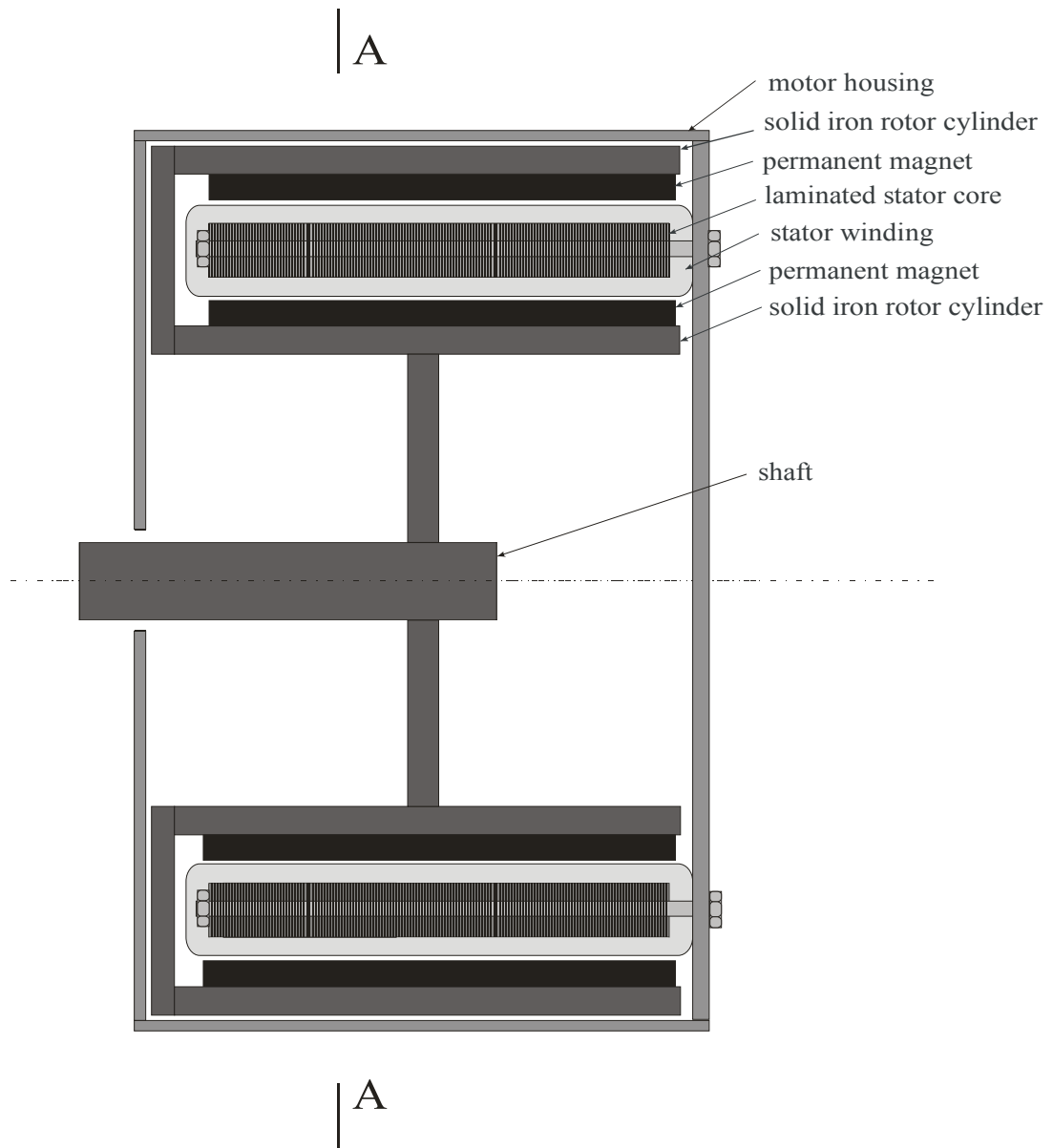
(a)

Figure 2.12: Scheme of radial flux twin rotor permanent magnet motor: (a) perpendicular cross-section, (b) longitudinal cross-section

(Figure continued)
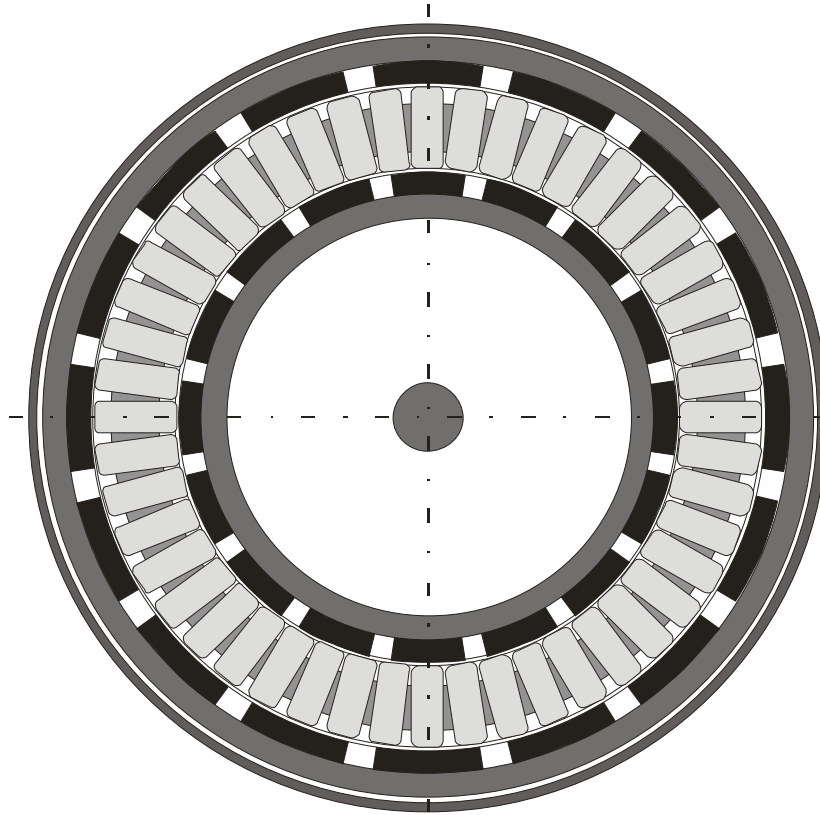
(b) A - A

The coils are connected in the three phase system as shown in Figure 2.13.

A1 C2 B1   A2 C1 B2
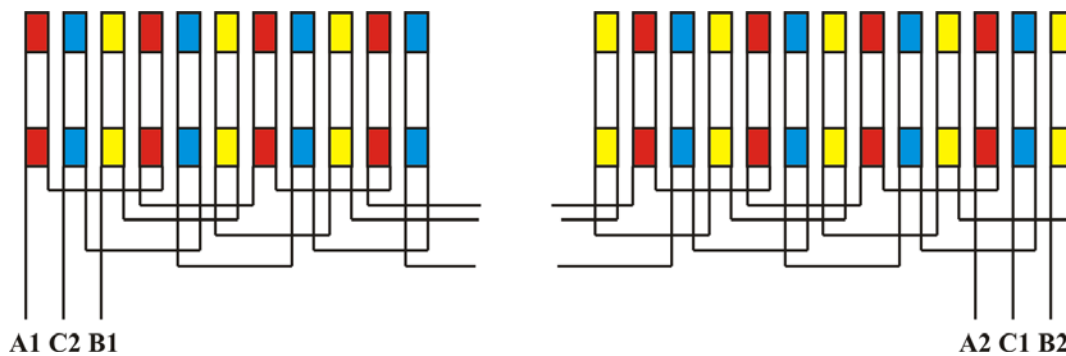
Figure 2.13: Three phase winding arrangement of the RFTR PM motor

The torque of a conventional RFPM machine is scaled as the square of the diameter times the length while that of an AFTR PM machine scale as the cube of the diameter. Hence, the benefits associated with axial flux geometries may be lost as the power level or the geometric

ratio of the length to diameter of the motor is increased. The transition occurs near the point where the radius equals twice the length of RFTR PM machine [7]. In such cases, clearly the radial flux motor may be preferred for higher power generation than a single stage axial flux motor. However, the comparative studies that are carried on cylindrical and multi-layer disc-type motors having the same volume indicate that the values of torque and consequently, of the output mechanical power, are higher in multi-layer disc-type motors [9]. The applications of radial flux motors are limited due to the following reasons:

- the bottle-neck feature for the flux path at the root of the rotor tooth in the case of the induction and dc brushless machines with external rotors

- much of the rotor core around the shaft is hardly utilized as a magnetic circuit

- heat from the stator winding is transferred to the stator core and then to the frame, that is, there is poor heat removal through the stator air gap, rotor and shaft without forced cooling arrangements.

In general, the special properties of AFTR PM machines, which are considered advantageous over conventional RFPM machines in certain applications, can be summarized as follows [7]:

- AFTR PM machines have much larger diameter to length ratio than RFPM machines

- AFTR PM machines have a planar and somewhat adjustable air gap

- Capability of being designed to possess a higher power density with some saving in core material

- The topology of an AFTR PM machine is ideal to design a modular machine in which the number of same modules is adjusted to power or torque requirements

- The larger the outer diameter of the core, the higher the number of poles that can be accommodated, making the AFTR PM machines a suitable choice for high frequency or low speed operations.

The above comparison is made between the conventional RFPM machine and AFPM machine. The comparison between the AFTR PM machine and the newly proposed RFTR PM machine will be done after the analysis of motor performance in the following chapters.

CHAPTER 3: FINITE ELEMENT METHOD (FEM) FOR ELECTROMAGNETICS

The finite element analysis is a flexible, reliable and effective method for the analysis and synthesis of power-frequency electromagnetic and electromechanical devices. The Finite Element Method (FEM) packages that are now available are user friendly and eliminate need of performing numerous calculations, to determine the electromechanical parameters, by using the analytical or semi-empirical formulae. These packages thus provide a simple way to obtain the electromagnetic field distribution and integral parameters to the user even without having the knowledge of applied mathematics.

3.1 Finite Element Method Magnetics (FEMM) [10]

FEMM [10] is a suite of programs for solving low frequency electromagnetic problems on two-dimensional planar and axisymmetric domains. FEMM may be divided into three parts: interactive shell (femm.exe), mesh generator (triangle.exe) and the solvers.

- The interactive shell is a multiple document interface which consists of a pre-processor and a post-processor. The pre-processor may be used for laying out the geometry of the problem to be solved and for defining the material properties and boundary conditions. The post-processor displays the field solutions in the form of contour and density plots, also allowing the user to inspect field at arbitrary points and plot various quantities of interest along user-defined contours. The results can be post-processed in order to derive the machine integral quantities and associated parameters.

- The mesh generator breaks down the solution region into large number of triangles which is a vital part of the finite element process, that is, FEMM discretizes the problem domain using triangular elements. The solution is approximated by a linear interpolation of the values of potential at the three vertices of the triangle of each element. The advantage of

breaking the domain into a number of small elements is that the problem becomes transformed from a small but difficult to solve problem into a big but relatively easy to solve problem.

- The data files that define the problem are acquired by each of the solvers and it solves the relevant Maxwell's equations to obtain values for the desired field throughout the solution domain.

The magnetics problems solved by FEMM are low frequency problems, in which displacement currents can be ignored. These currents are relevant to magnetics problems at radio frequencies. The converse is true for electrostatic problems, where the electrostatics solver considers only the electric field and magnetic field is neglected.

- **Maxwell's equations:**

For magneto static problems in which fields are time-invariant, the field intensity H and flux density B must obey:

$$\nabla \times H = J \tag{3.1}$$

$$\nabla \cdot B = 0 \tag{3.2}$$

The field intensity and flux density of a material may be related as:

$$B = \mu H \tag{3.3}$$

FEMM finds a field that satisfies the above the equations (3.1), (3.2) and (3.3) via a magnetic vector potential approach. The flux density may be written in terms of the vector potential, A as:

$$B = \nabla \times A \tag{3.4}$$

This definition of B always satisfies equation (3.2) and hence equation (3.1) can be rewritten as:

$$\nabla \times \left(\frac{1}{\mu(B)} \nabla \times A \right) = J \tag{3.5}$$

The Finite Element Method Magnetics retains the form of equation (3.5) so that magnetostatic problems with a nonlinear B-H relationship can be solved. In the general 3-D case, A is a vector with three components. However, in the 2-D planar and axisymmetric cases, two of these three components are zero, leaving just the component in the "out of page" direction. The advantage of using vector potential formulation is that all the conditions to be satisfied have been combined into a single equation. If A is found, B and H can then be deduced by differentiating A.

3.2 Description of FEMM 4.0 Program

The version 4.0 of Finite Element Method Magnetics (FEMM) package is used in this thesis. The parameters of the three-phase permanent magnet brushless disc type and cylindrical shape twin rotor motors are obtained by using the two-dimensional finite element method. For this purpose, first, a model of each of the motors to be analyzed is to be drawn in the interactive shell of the FEMM 4.0 software. In other words, the outline, dimensions and materials of the motors are to be specified on a 2-D plane. As said earlier, the interactive shell consists of preprocessor and postprocessor drawing modes.

- **Preprocessor drawing modes:**

The preprocessor is always in one of the five modes: Point mode, Segment mode, Arc Segment mode, Block mode, Group mode. The point mode is used to pin nodes that define all corners of the geometrical model. The segment or arc segment mode may be used to join the nodes with line segments or arcs respectively. The block mode helps to define the materials and their properties in each solution region. The group mode glues different objects together into parts so that entire parts can be manipulated more easily. The default drawing mode is the point mode, but it is easy to switch between the different modes by just clicking on the corresponding mode. Figure 3.1 shows all these modes.
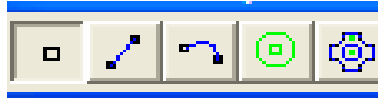
Figure 3.1: Preprocessor drawing mode toolbar buttons

The user can size or move the view of problem geometry displayed on the screen by using the view manipulation toolbar buttons shown in Figure 3.2. The four arrow buttons help to move the view in the direction of the arrow approximately half of the current screen width. The "+" and "-" buttons zoom in and zoom out the current view. The screen can be scaled to fit the entire problem geometry by using the "blank page" button. To zoom a specific part of the screen, the "page with magnifying glass" button may be used.
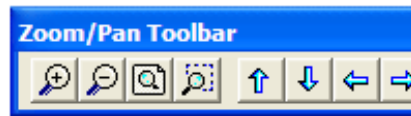
Figure 3.2: View manipulation toolbar buttons

The grid manipulation toolbar buttons (Figure 3.3) may be used to display or hide the grid on the screen, to specify the grid size and to snap the pointer to the closest grid point. The coordinates defining the problem may be specified in cartesian or polar form.
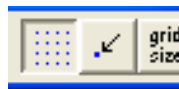
Figure 3.3: Grid manipulation toolbar buttons

An existing geometry may be modified by using the editing buttons provided on the toolbar. The last addition or deletion to the model's geometry may be undone by using the "undo" button. A region may be selected by dragging the pointer over the specified area and performing operations like moving, copying, scaling or deleting the selected area is simple. The selected objects may be horizontally or vertically displaced and may be rotated according to our necessity. These icons are shown in Figure 3.4.
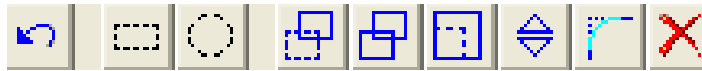
Figure 3.4: Toolbar buttons for editing operations

For creating geometry, the problem has to be defined by using the "Problem Definition" dialogue box. The problem type (planar or axisymmetric), length units, frequency, depth (length of geometry in the "into the page" direction), solver precision and the minimum angle for the triangle meshing can be specified before drawing the model of the problem to be solved. To make a solvable problem definition, the user must define the properties of the material used in each solution region and identify the boundary conditions by specifying the properties of line segments or arcs that are to be the boundaries of the solution domain. The existing materials may modified or deleted later and new properties may be added at any time. The material can be chosen to have a linear or non-linear B-H curve according to the requirement of user. Similarly, the current density, electrical conductivity and special attributes like lamination and wire type may be specified. The user can access and add materials to his model from the materials library. The circuits in model can be defined as parallel or series and the circuit current can be assigned.

Triangular mesh can be created over the whole model at a single click and the model can be simulated or analyzed using the "hand-crank" icon on the toolbar. Figure 3.5 shows these icons. The solution time varies depending on the size and complexity of the problem. Generally, linear magneto static problems take the least amount of time. The slowest problems to analyze are nonlinear time-harmonic problems, since multiple successive approximation iterations must be used to converge on the final solution. The "big magnifying glass" icon is used to display the results in a post processing window once the analysis is competed.

Figure 3.5: Analysis toolbar buttons

- **Postprocessor modes:**

Like the preprocessor, the postprocessor can be operated in the point mode, contour mode or the block mode and the view manipulation toolbar buttons can be put to use as needed. The additional icons in this mode are the graph mode toolbar buttons (Figure 3.6), which can be used to obtain the plots to display the results. The flux lines can be viewed over a specified contour of the model by using the "contour plot" icon. The user can choose to plot the flux density or current density with the help of "density plot" icon and the "vector plot" icon is a good way to get an indication of the direction (by arrows) and magnitude of the field.

Figure 3.6: Graph mode toolbar buttons

The values of the desired quantities are computed and X-Y graph is plotted by the "line plot" icon. The integral values of certain parameters over a defined closed contour can be obtained by using the "integral" icon on the toolbar. If circuit properties are used in the model, then a number of useful properties relative to the circuit are automatically available in the postprocessor mode and they can be viewed using the "circuit results" icon. These icons are illustrated in Figure 3.7.
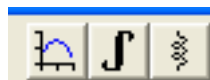
Figure 3.7: Line plot, integration and circuit results toolbar buttons

To summarize, the various steps in constructing a model and obtaining the results are as follows:

1) Specify the problem definition and draw the model using nodes, line and arc segments.

2) Assign block labels to each solution region, add materials and define the properties of materials.

3) Provide the circuit properties to model and assign the circuit currents.

4) Define and apply boundary conditions.

5) Analyze the problem and view results.

6) Graphs may be plotted with a legend, to illustrate the results obtained and values of various electromechanical parameters may be noted down.

FEMM 4.0 is user friendly software to create the model of the problem to be solved and to analyze it. The results are obtained in a few simple steps, as described in this chapter.

CHAPTER 4: DISC-TYPE DOUBLE-ROTOR PM BRUSHLESS MOTOR: OPTIMIZATION OF CORE DIMENSIONS AND DETERMINATION OF ELECTRO-MECHANICAL PARAMETERS

This chapter gives an insight into the design specifications of one of the objects of the thesis, the disc type twin rotor brushless PM motor. The objective of this chapter is to optimize the thickness of stator and rotor core for the given main dimensions of the motor and the winding data. Having this data, the next objective is to determine winding resistance and inductance and the torque for the given supply voltage and current. To do this, a FEMM model is developed.

4.1 Design Data of the Motor

The disc type motor to be analyzed is a three phase motor with sixteen magnetic pole pieces on the rotor. The stator winding carries fourteen turns per coil on each phase. Figure 4.1 (a) shows the base data marked on the model of the disc type twin rotor PM motor. The angle subtended by each magnetic pole piece and the three phase winding at the shaft of the motor is indicated in Figure 4.1 (b).

The rotor is made of steel and the stator is laminated. The rotor speed, thickness of permanent magnets on the rotor and the details of the winding on the stator are provided. Table 4.1 gives the data for the disc type double-rotor permanent magnet motor whose performance is to be evaluated.

The parameters of the disc type motor to be evaluated, using the data provided above, are as follows:

- **Design parameters to optimize:**

    - Thickness of the stator core (laminated steel)

    - Thickness of the rotor discs (solid iron)
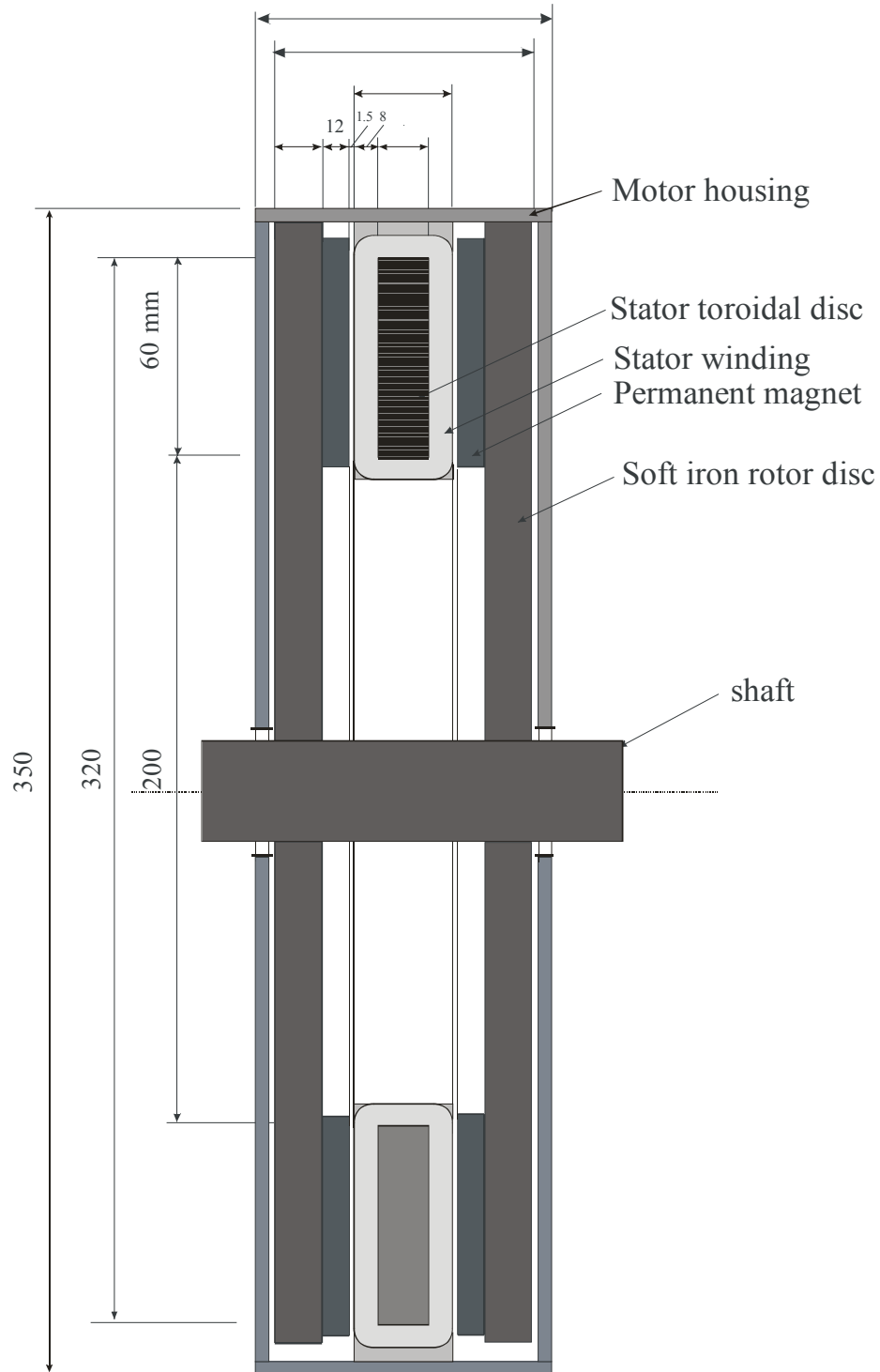
Figure 4.1 (a): Disc type double-rotor PM motor with the base data indicated

22.5 deg

20 deg

12 mm
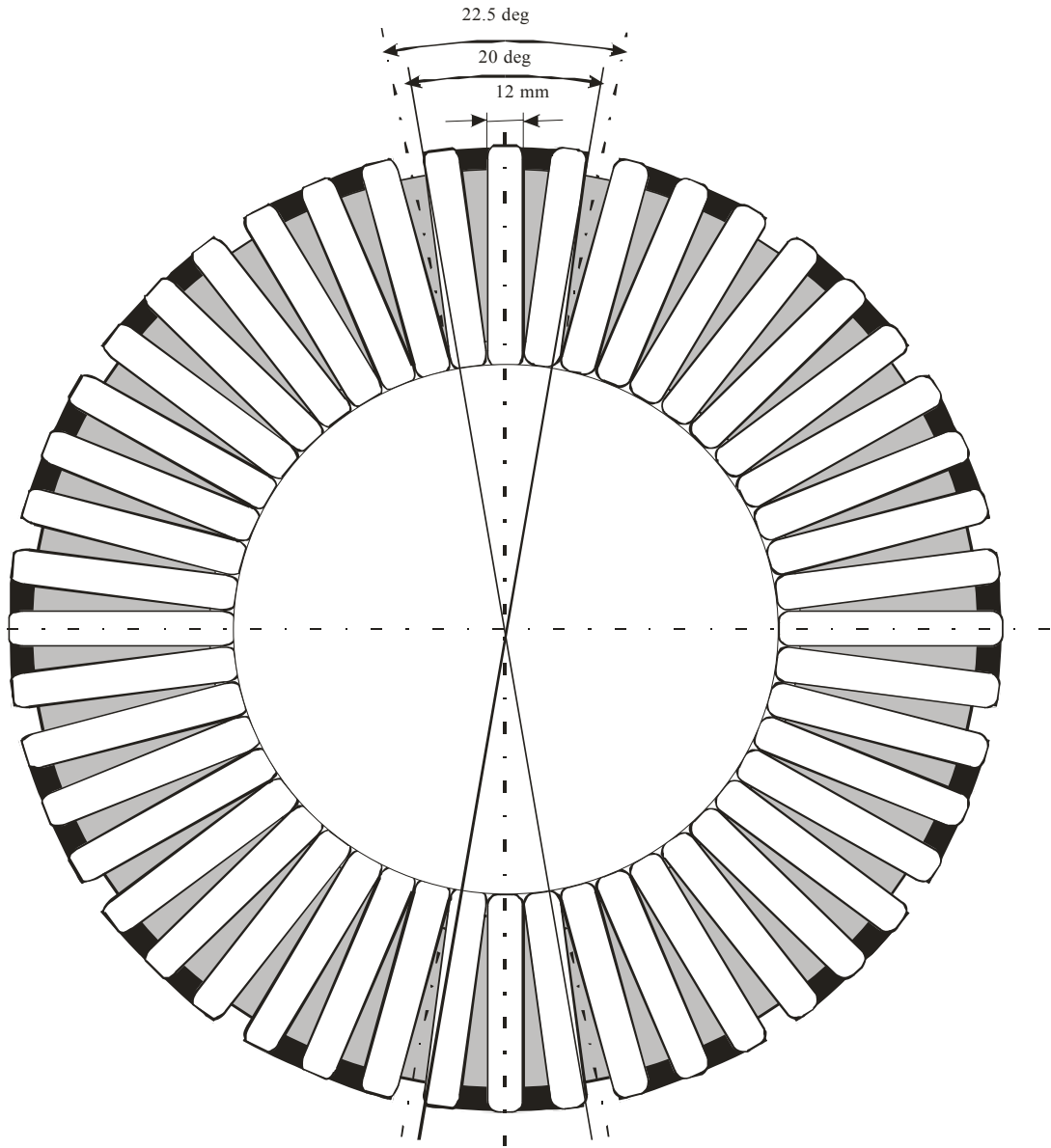
Figure 4.1 (b): Trapezoidal magnetic pole pieces and stator coils

Table 4.1: Specifications for the disc type double-rotor PM motor

Assumed data	
Magnetic pole number	16
Winding:	
- Number of phases	3
- Number of coils/phase/pole	1
- Coil number	48
- Turn number/coil	14
- Wire diameter Dw	AWG11 – Dw=2.30378mm
- Coil cross-section area Ac=12x8	96 mm2
- Wire cross-section area Aw	4.168 mm2
- $k_{Cu} = \dfrac{A_w \times N_w}{A_C} = \dfrac{4.168 \times 14}{96} = 0.608$	
Rotor speed	822 rpm (86.08 rad/s)
Magnet thickness	12 mm
Flux density in the rotor discs (permissible)	1.5 T
Flux density in the stator discs (permissible)	1.8 T
Rotor core	Steel 1117 (Figure 4.2 (a))
Stator laminated core	US Steel type 2-S, 0.018 inch thickness(Figure 4.2 (b))
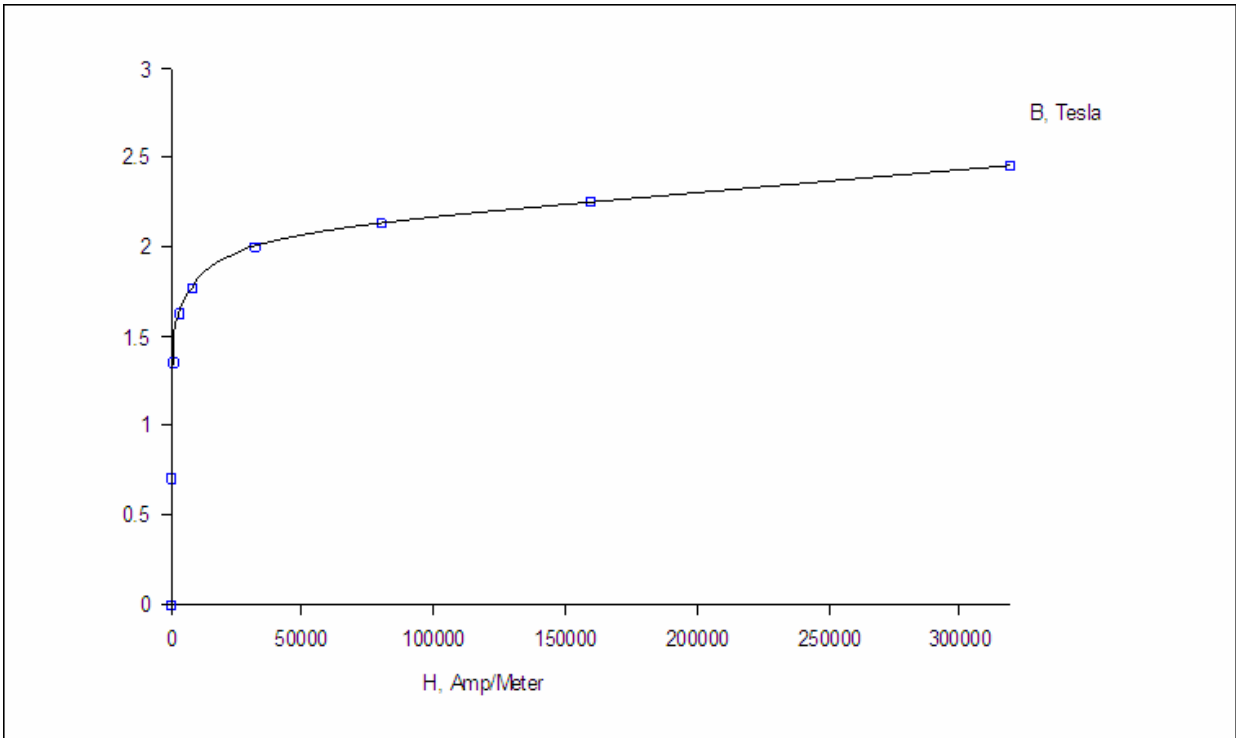
(a)
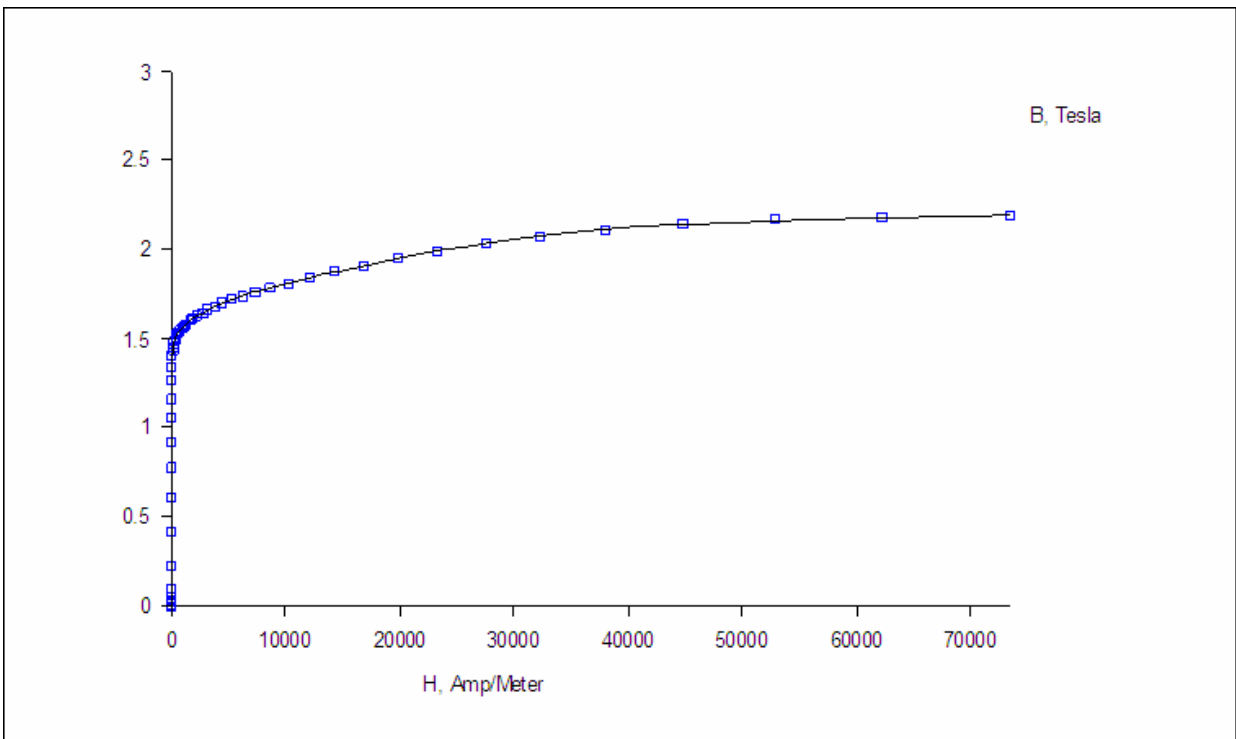
(b)

Figure 4.2: Magnetization characteristic of (a) rotor core, (b) stator core

- **Electromechanical parameters to determine:**

  - Electromagnetic torque

  - Electromotive force

  - Resistance

  - Self inductance

  - Mutual inductance

  - Voltage across terminals

4.2 Motor Model and Simulation in FEMM 4.0

In order to analyze a magnetic field of the disc motor, a 3-D motor model has to be used. Since the FEMM 4.0 software allows calculating in 2-D space, the actual motor had to be modified to the flat model, in which all curvatures are developed with respect to the average radius placed in the middle of the stator core.

With the data provided on the angle subtended by the magnetic poles at the center of motor, the length of each magnet piece and the distance between two adjacent pieces is calculated. In a similar way, the length of the coil winding on the stator for each phase and the distance between two phases is obtained. The motor model is developed in FEMM 4.0 and the thickness of rotor and stator are adjusted such that the desired flux density is achieved in them. The corresponding materials and circuit currents are assigned to each block of the model as shown in Fig 4.2. Since the 2-D model of the motor is symmetric, the FEMM model is created for eight magnetic pole pieces and for one rotor. The calculation results obtained from this model may be later manipulated to obtain the values for the entire motor. However, Figure 4.2 indicates only a part of the FEMM model. With this working model of disc motor, calculations were carried out and the results are discussed in the following sections of this chapter.
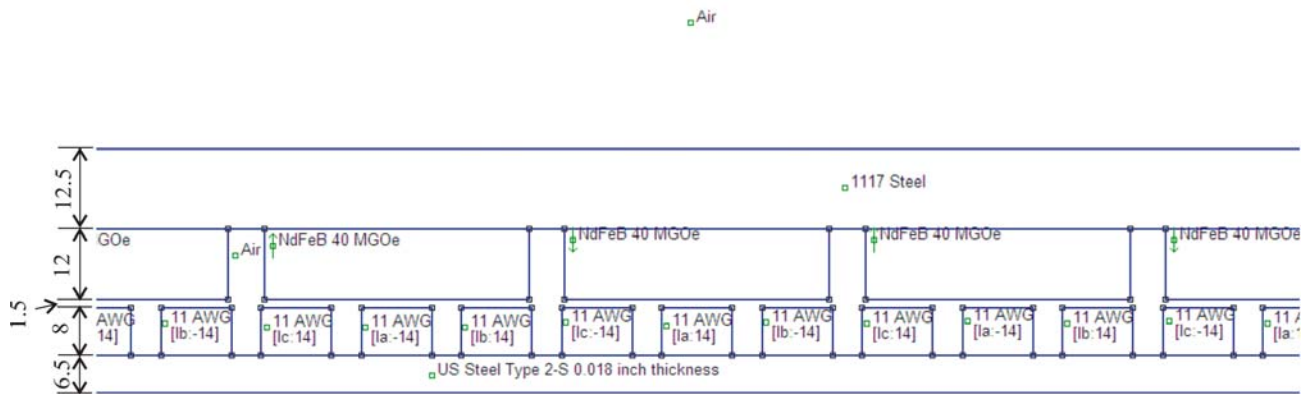
Figure 4.3: FEMM 4.0 model for the disc motor

4.3 Magnetic Flux Distribution

The magnetic flux density distribution in the motor plays a decisive role in the electromagnetic torque developed by the motor. Thus it is necessary to determine it and to examine how the stator current influences it. Figure 4.4 shows the current distribution and magnetic field lines generated by the permanent magnets and currents for a particular time instance. The relatively symmetrical distribution of the magnetic field lines with respect to the radial symmetrical axis of the magnets indicates a negligible influence of currents on resultant magnetic field.

In Figure 4.5, a magnetic flux density distribution is shown for the case when the angle between the rotor flux vector and current vectors equals 90°. The current vector is equal to the rated current in both diagrams (Figure 4.4 and Figure 4.5). The maximum flux density is higher in stator core than in the rotor because the stator core is made of laminated steel which goes into saturation at much higher values (see Figure 4.2 (b)).

37
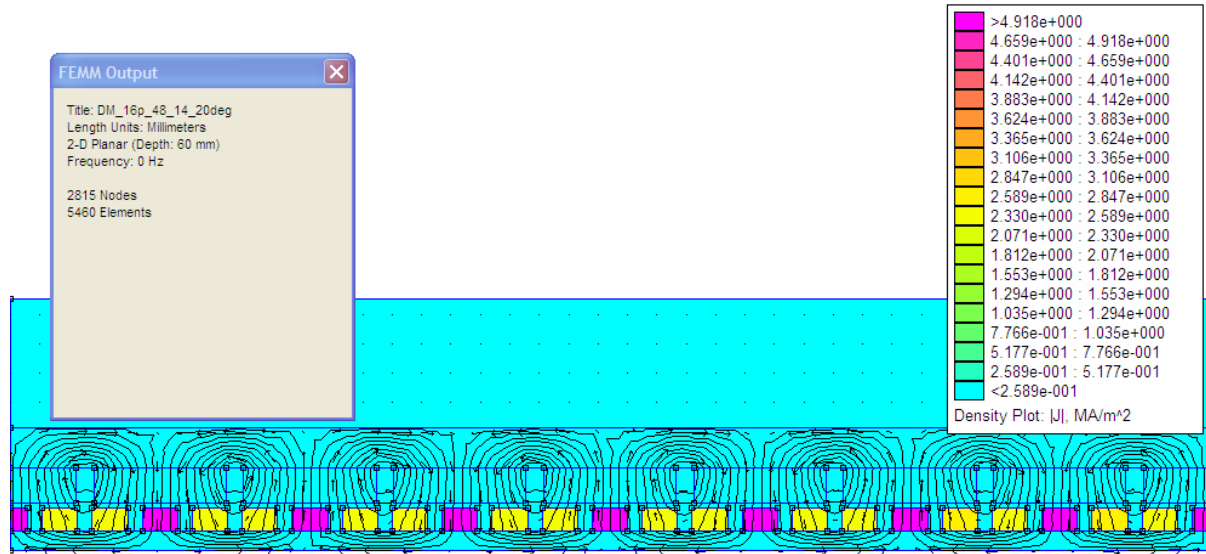
Figure 4.4: Current density and magnetic field lines plot for the disc type motor
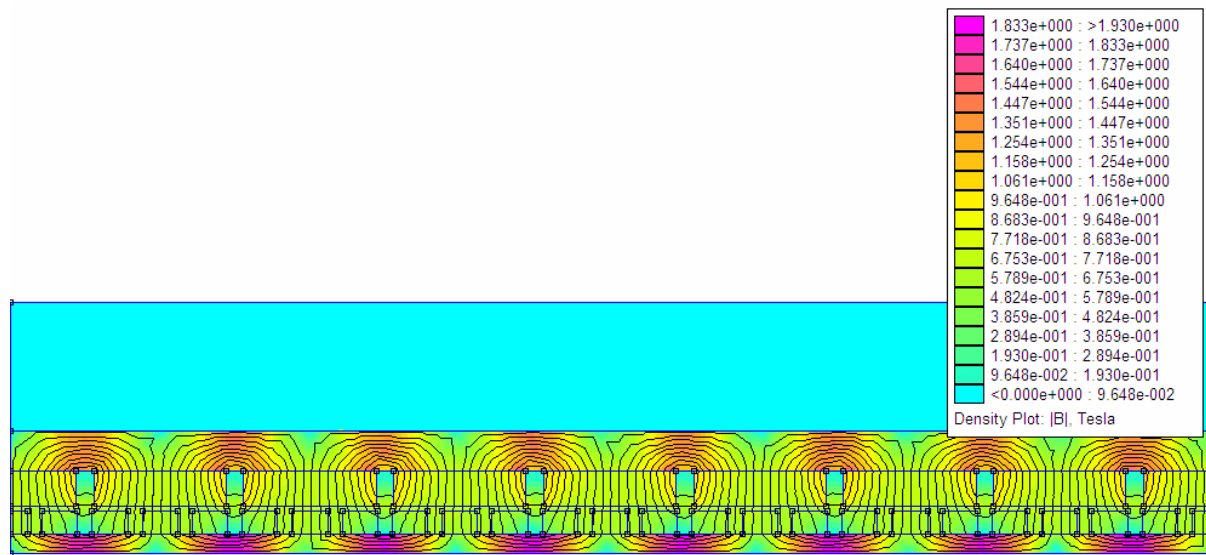
Figure 4.5: Flux density distribution for the disc type motor model

To show how the position of the stator with respect to the rotor influences the magnetic flux density distribution in the motor, calculations were done at three different angles between the rotor flux vector and current space vector equal to $90°$, $60°$ and $30°$. The results are presented in Figure 4.6.
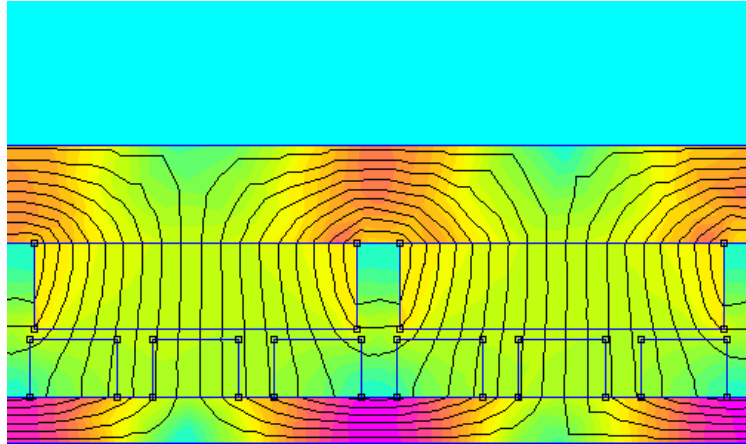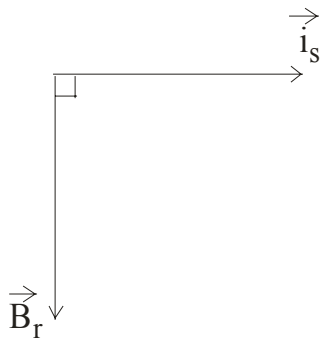
(a)
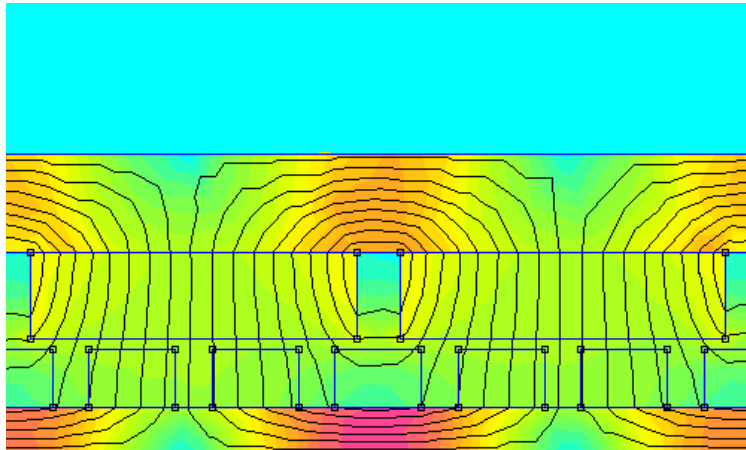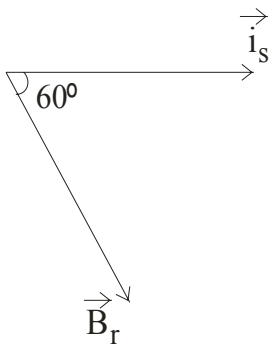
(b)
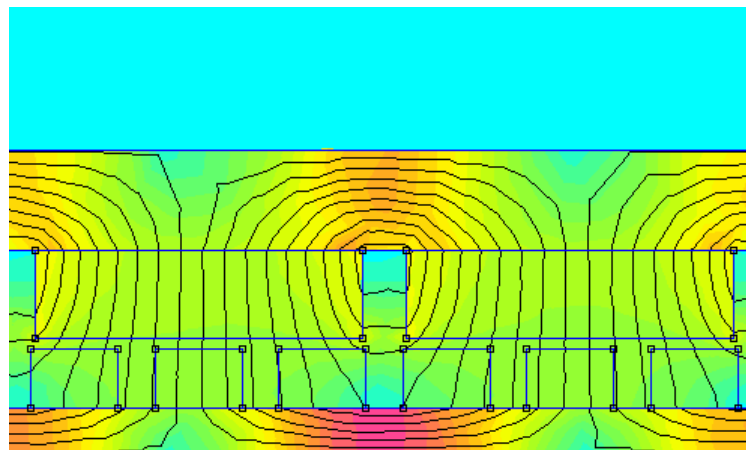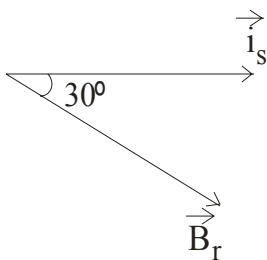
(c)

Figure 4.6: Flux density plots for the power angle of: (a) 90°, (b) 60° and (c) 30° degrees

In Figure 4.7 are the plots for the normal component of the magnetic flux density determined in the air gap between permanent magnet and stator winding over the length of one pole pitch. These characteristics were determined for the same conditions as those in Figure 4.6.
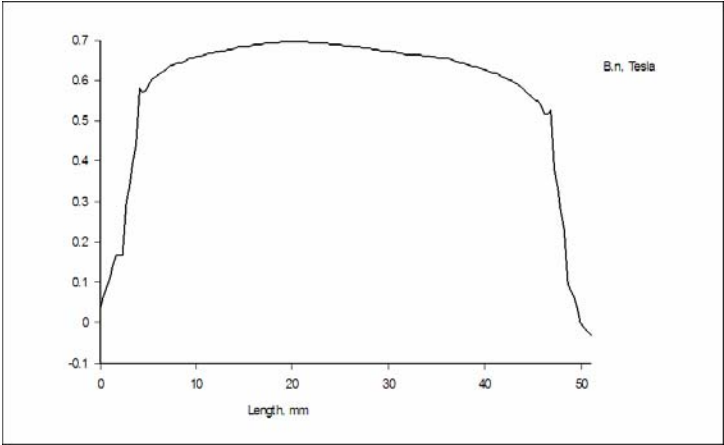
(a)
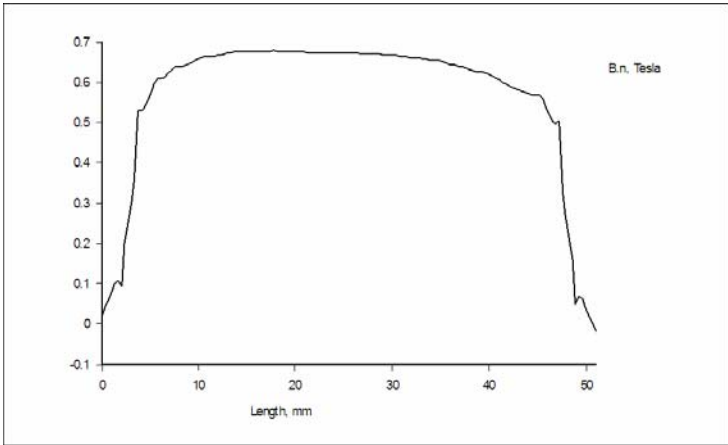
(b)

Figure 4.7: Magnetic flux density distribution in the air gap for power angle of: (a) 90°, (b) 60° and (c) 30°

(Figure continued)
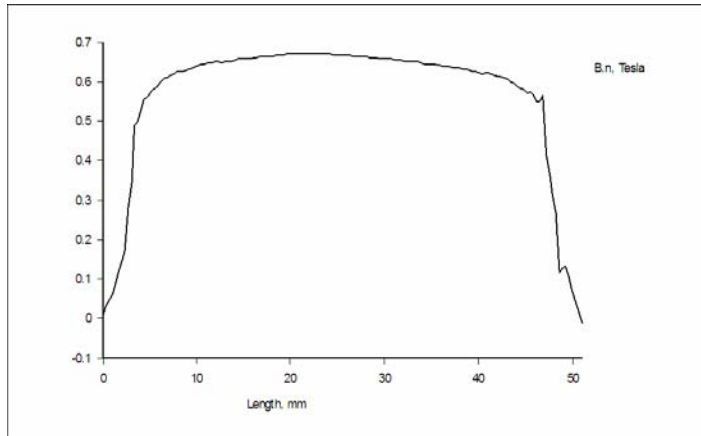
(c)

The presented results show negligible influence of magnetic flux generated by currents on PM flux. More visible changes are on Figure 4.7. The flux density distribution has different values at the edge of magnets. For absence of currents in the winding, the distribution of flux density would be symmetrical.

4.4 Determination of Motor Parameters

4.4.1 Stator and Rotor Thickness

Considering the fact to stick to the values of permissible magnetic flux densities, the thickness of each of the rotor discs of the disc type twin rotor motor is found to be 12.5 mm and that of stator as 13 mm. These values are obtained by changing the FEMM model until a magnetic flux density value of 1.5 T is achieved in the rotor and a value of 1.8 T is attained in the stator core. It is assumed that above these values, both stator and rotor cores are saturated (see Figure 4.2).

4.4.2 Stator Winding Parameters

- **Phasor resistance**

The phase resistance of the stator winding coil is calculated with the help of data provided and by using the following formula:

41

$$R = L_{c,av} \times N_W \times N_C \times R_{awg} \qquad (4.1)$$

where $L_{c,av}$ is the average length of the coil in km

N_W is the number of turns per coil

N_C is the number of coils per phase

R_{awg} is the resistance per kilometer of the AWG wire [11]

For the values of $L_{c,av}$=171 mm, N_W=14, N_C=16 and R_{awg}=4.1328 Ω, the phasor resistance of the stator coil winding is found to be R = 0.1584 Ω.

- **Self inductance**

The self inductance of each phase of the stator winding is calculated by following a simple procedure and the FEMM model of the disc motor. First, the permanent magnets on the rotor are changed to air and the current is assigned only to the phase whose self inductance is to be found. The other phases are given a zero current. The FEMM model is then analyzed and the flux/current value for I_a is noted down by clicking on the circuit icon. This value indicates the self inductance value for the stator coils under eight magnetic pole pieces. Hence, the value obtained is doubled. It is further multiplied by 2 (the second side of the motor) to obtain the self inductance of the phase considered.

$$L = (flux / current) \times 2 \times 2 \qquad (4.2)$$

where L is the self inductance.

The results achieved are as follows:

Self inductance of phase A, L_A = 0.2863 mH

Self inductance of phase B, L_B = 0.2925 mH

Self inductance of phase C, L_C = 0.2927 mH

- **Mutual inductance**

The procedure followed to obtain the mutual inductance between any two phases of the stator winding is almost similar to that followed for calculating the self inductance values, except for a few modifications. First, the permanent magnets on the rotor are changed to air as done before. For calculating the mutual inductance between phases A and B, the current is assigned only to phase A and the currents in phase B and phase C are zero. The motor model is then analyzed and the flux linkage value for winding I_B is read by clicking the circuit icon. This flux linkage value is divided by current I_A, which is then multiplied by 4. This gives the mutual inductance between phases A and B. A similar procedure is followed to obtain the mutual inductance value between the other phases.

$$M_{AB} = \frac{flux\ linkage}{I_A} \times 4 \tag{4.3}$$

where M_{AB} is the mutual inductance between phase A and B.

The values obtained are indicated below.

Mutual inductance between phase A and phase B, $M_{AB} = 0.1015$ mH

Mutual inductance between phase B and phase C, $M_{BC} = 0.1025$ mH

Mutual inductance between phase C and phase A, $M_{CA} = 0.1011$ mH

- **Synchronous inductance**

The synchronous inductance is a sum of the average self inductance and a half of the average value of mutual inductance.

$$L_s = L_{av} + \frac{1}{2} M_{av} \tag{4.4}$$

The value of synchronous inductance obtained in this method is $L_s = 0.3418$ mH.

4.5 Electromagnetic Parameters of the Motor

The variation of torque and emf with the change in rotor angle is observed and plots are made for the same.

4.5.1 Electromagnetic Torque

An interaction of normal component of the magnetic field and stator current contributes to the electromagnetic torque. The value of the torque is proportional to the current i and flux density B according to the following equation:

$$T_{em} = K_T B(\theta) \times i(\theta) \tag{4.5}$$

Both current and flux are function of space angle θ. Since the distribution of magnetic flux and current along the stator periphery varies, the torque developed by the motor will vary too if the rotor would change its position with respect to stator. To examine this variation, three cases are considered:

1) Phase A is supplied by the constant current of 35.5A, while the currents in phases B and C are equal to zero.

    The rotor position is changing starting from angle $\theta = 0^\circ$ (see Figure 4.8). Using the FEMM model, the Lorentz's Force F_{em} is calculated at different angle θ and then the torque is calculated from the equation given below:

$$T_{em} = F_{em} \times 4 \times r_{av} \tag{4.6}$$

where $r_{av} = 0.16$ m is the average radius of the stator core.

The electromagnetic torque determined in this way is plotted in Figure 4.9. This is the characteristic of torque developed by a single phase for the constant current value. The torque changes nearly sinusoidally because there are no slots in the stator core.
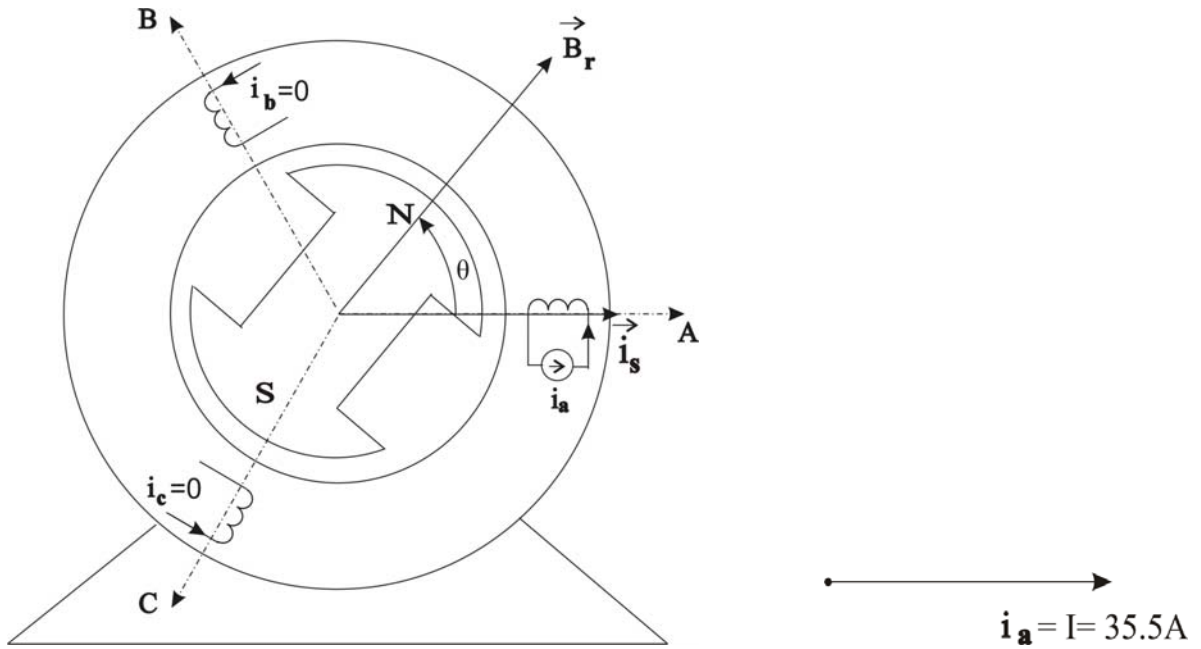
Figure 4.8: Rotor position and stator winding currents for case 1
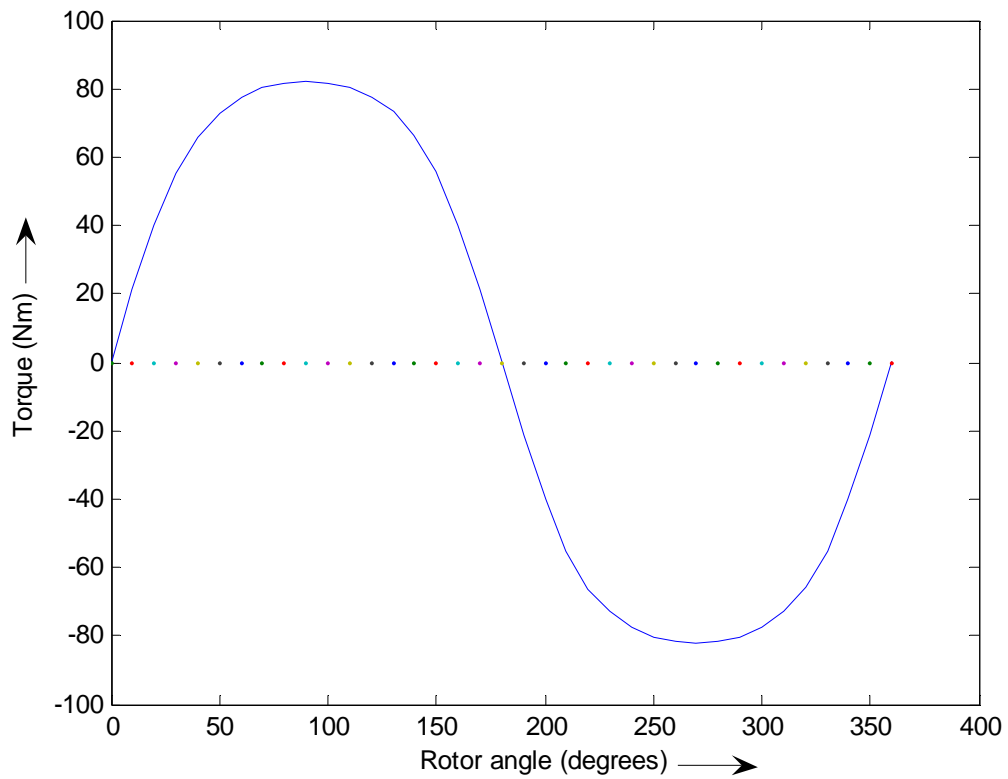
Figure 4.9: Electromagnetic torque developed by the rated current in phase A at different rotor positions

2) Phases A, B and C are supplied with the DC currents of 35.5A, -17.75A and -17.75A respectively according to the phasor diagram drawn for time instant t_1 as shown in Figure 4.10. The rotor is moving in positive direction.

   The torque is produced by the resultant current vector i_s and the characteristic $T_{em} = f(\theta)$ correspond to the torque-power angle characteristic known in the theory of synchronous motor [12].

   The torque - space angle characteristic determined in a similar way as that in Figure 4.9 is presented in Figure 4.11. This characteristic is nearly sinusoidal, which is the usually desired change in synchronous motors.
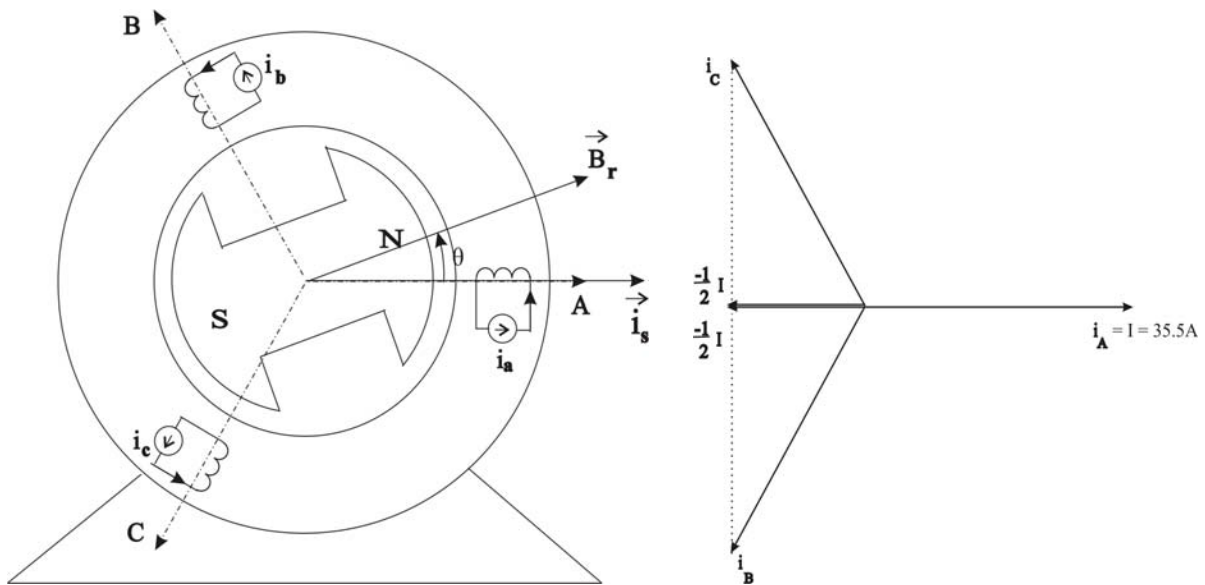
Figure 4.10: Rotor position and phasor diagram of stator currents at time instant t_1

3) Phases A, B and C are supplied by the three phase sinusoidal currents and the rotor flux B_r, displaced by 90° with respect to the current space vector i_s, moves synchronously as B_r, shown in Figure 4.12.
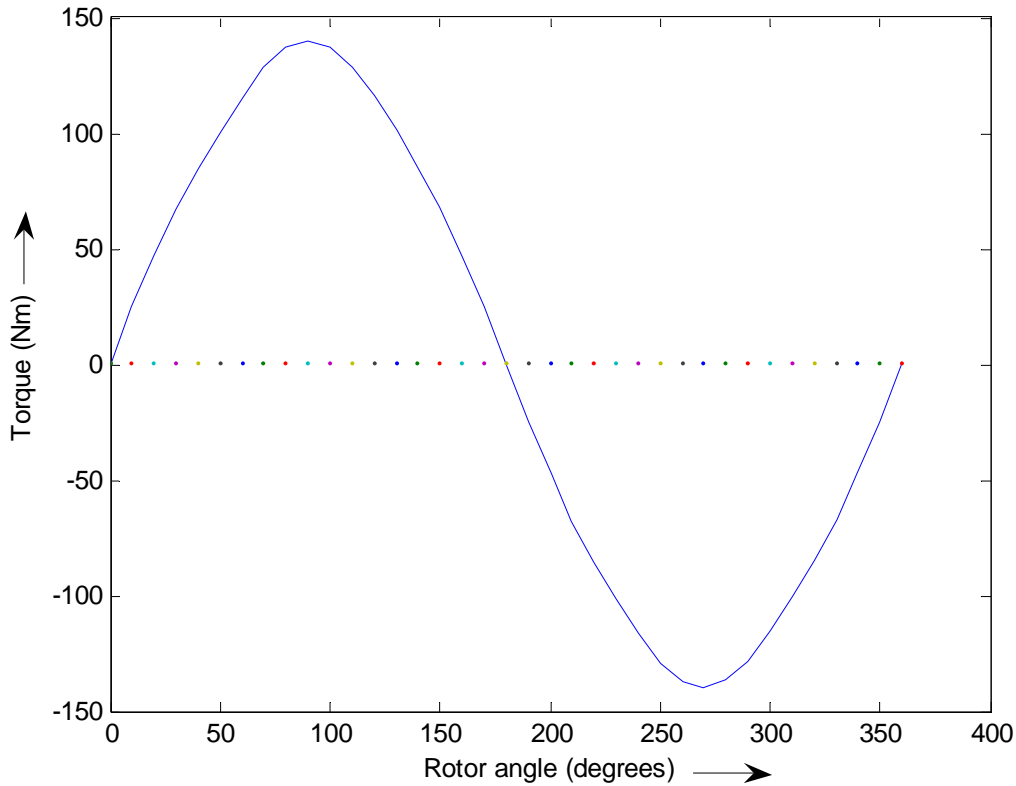
Figure 4.11: Electromagnetic torque developed by the motor at different rotor positions with respect to the stator current space vector

In this case, the rotor flux density vector and current vector move synchronously, being displaced from one another by 90°, as in brushless DC motors. The torque developed by such vectors changes with the position of both vectors. This change is shown in Figure 4.13.

Since the angle is changing in time, the characteristic can be regarded also as waveform of the torque of brushless DC motor. The torque as one can see changes within the range $134.5106 Nm \leq T_{em} \leq 139.9064 Nm$. This change is caused by not sinusoidally distributed stator winding. Thus, the torque ripple is negligible. In general, there is no cogging torque caused by slots in case of toothed stator core.
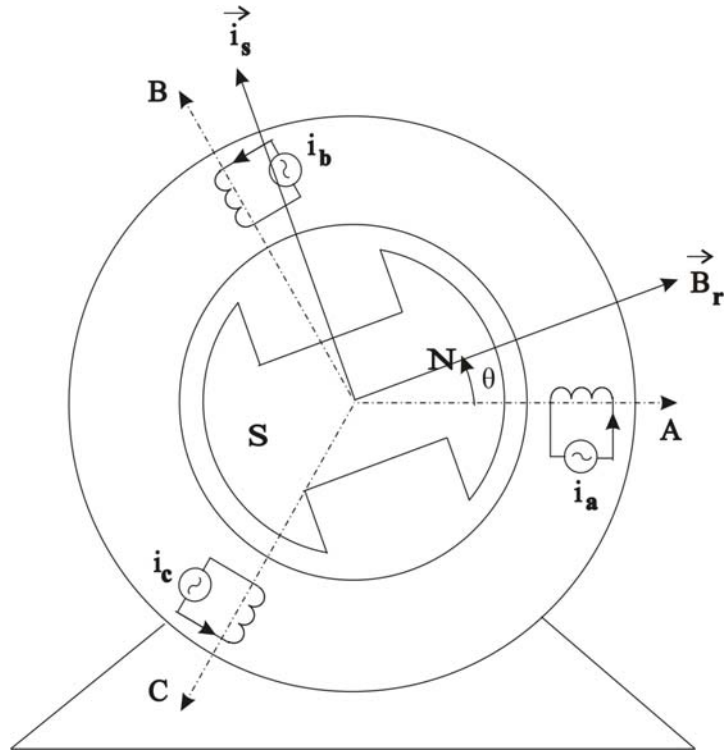
(a)
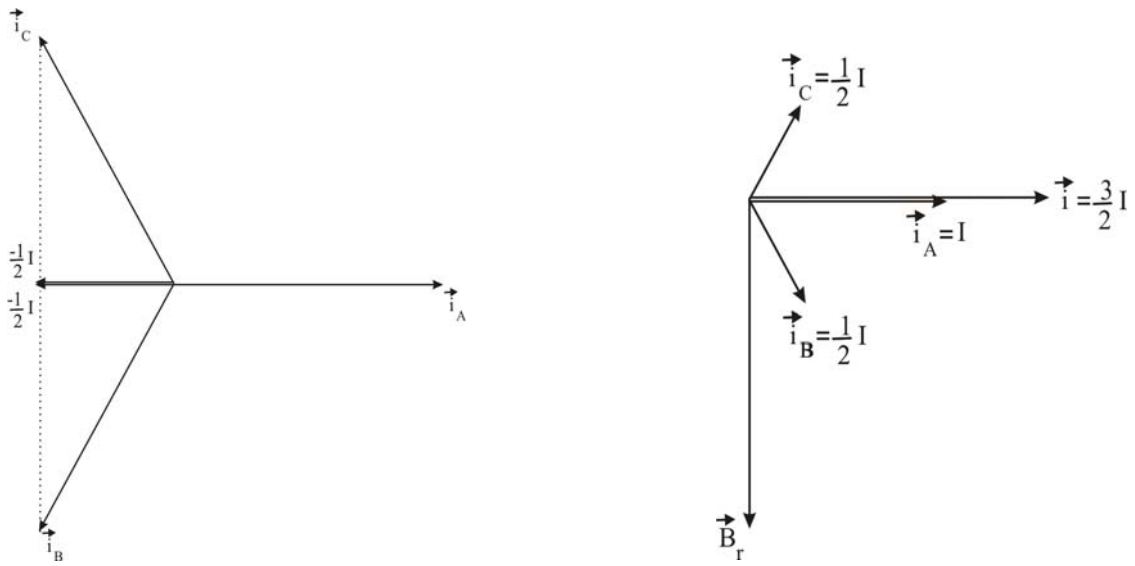
(b)

Figure 4.12: Change of space currents synchronously with rotor flux at two time instants t_1 and t_2

(Figure continued)

(c)
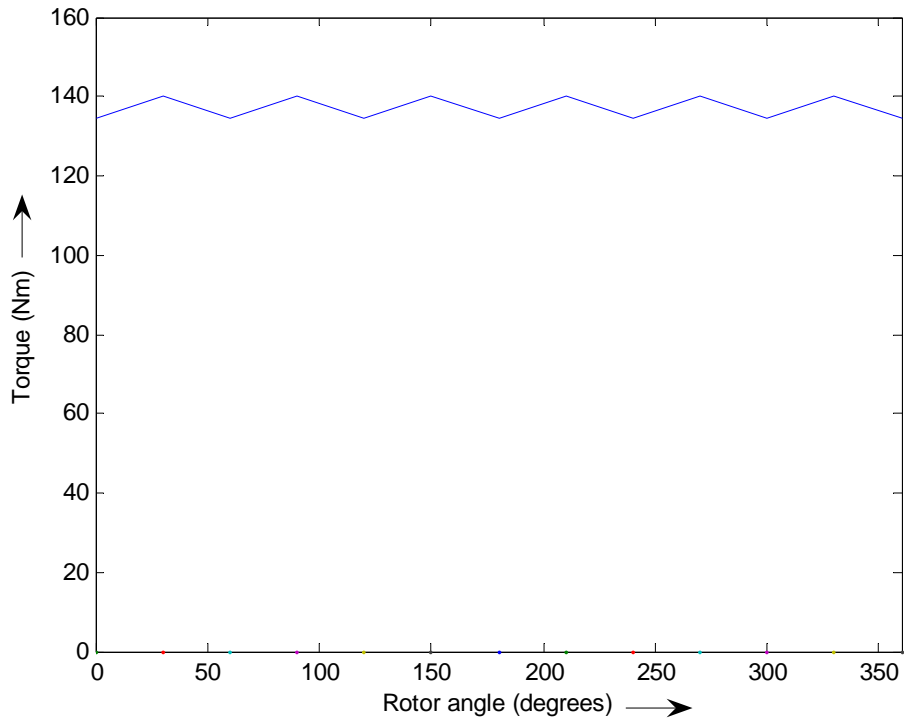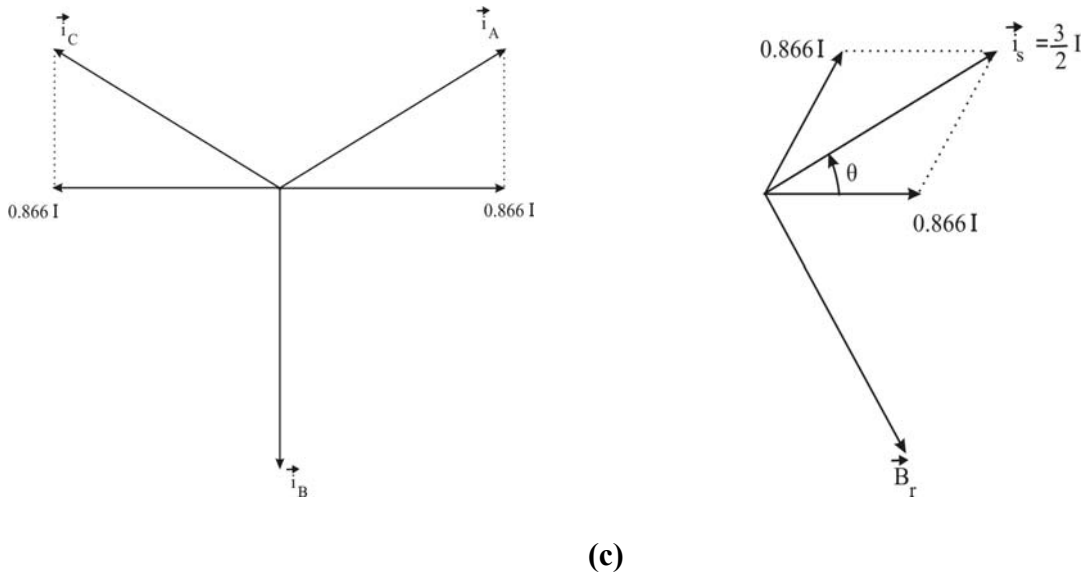
Figure 4.13: Electromagnetic torque vs. space angle θ determined at power angle (angle between current and rotor flux space vectors) of 90°

4.5.2 Electromotive Force

When the rotor magnetic flux rotates, it induces electromotive force (emf) in the stator winding. Thus, emf depends on rotor speed ω_m and flux linkage λ according to the following equation:

49

$$e = \omega_m \lambda(\theta) \qquad (4.7)$$

Since the torque depends also on flux linkage as $T_{em} = \lambda \times i_s$, the electromotive force of phase A can be determined from the torque using the relation given below:

$$e_{ph} = \omega_m \frac{T_{em,ph}}{i_{ph}} \qquad (4.8)$$

Using this procedure, the emf was determined for the phase A and its characteristic, as a function of space angle, is plotted as shown in Figure 4.14. This characteristic is similar to the emf waveform in case of constant stator speed.
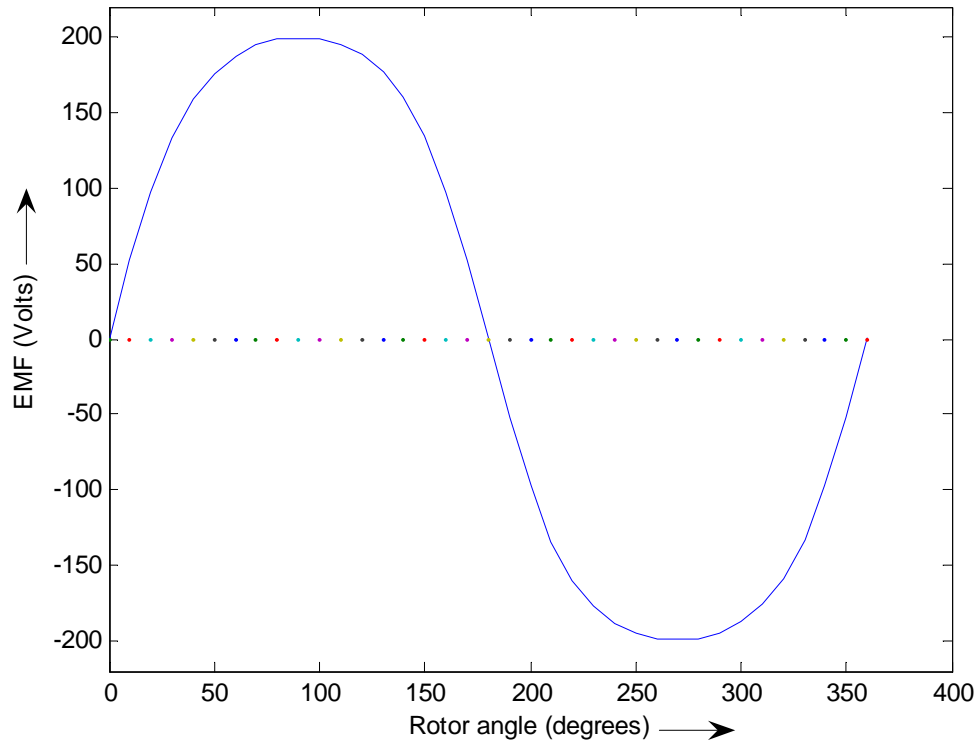
Figure 4.14: EMF induced plot as a function of space angle θ

4.5.3 Terminal Voltages

To determine the voltage across winding terminal, the equivalent circuit of synchronous motor is used which is shown in Figure 4.15.
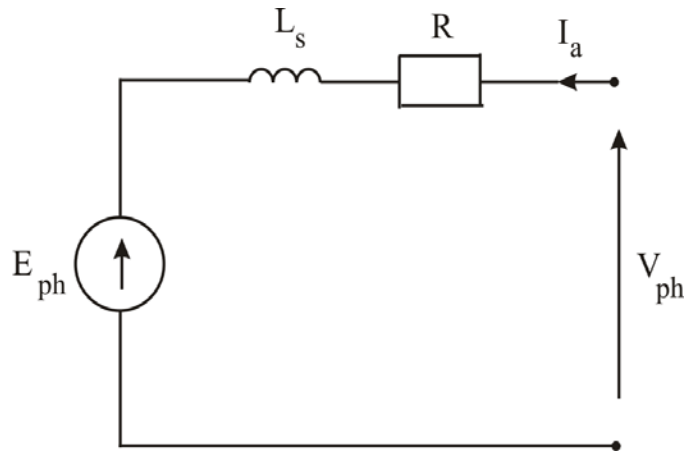
Figure 4.15: Equivalent circuit of synchronous motor

For PM motor operating as a brushless DC motor, the space vector diagram at t = 0 for R = 0 is as shown in Figure 4.16.
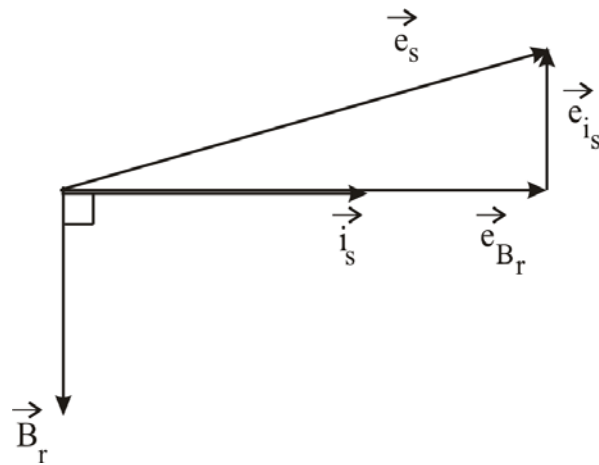
Figure 4.16: Space vector diagram at t = 0 and for R = 0

The phasor diagram of phase A related to the space vector diagram is shown in Figure 4.17.
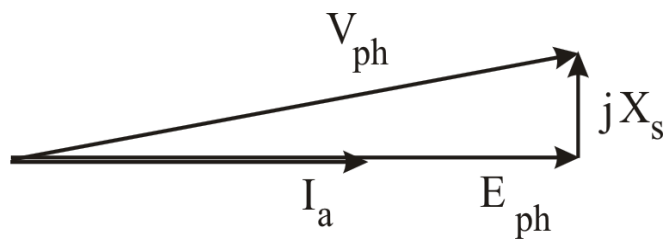
Figure 4.17: Phasor diagram of phase A

If the resistance is included, the corresponding phasor diagram looks like the one shown in Figure 4.18.
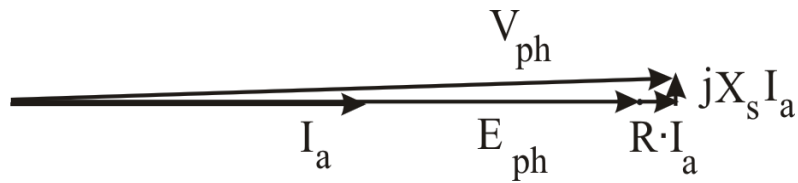
Figure 4.18: Phasor diagram with resistance included

The corresponding voltage equation is as follows:

$$V_{ph} = E_{ph} + RI_a + jX_s I_a \tag{4.9}$$

For the analyzed motor, the values of equivalent circuit parameters are:

$R = 0.1584 \ \Omega$

$L_s = 0.3418 \ mH$

For the rated speed $\omega_m = 86.08$ rad/sec, $\omega_e = \dfrac{p}{2}\omega_m = 688.6 rad/s$, $X_s = \omega_e L_s = 0.235\Omega$ the emf

$E_{ph} = 141$ V and for rated current $I_a = 35.5/\sqrt{2} = 25.10$ A,

$V_{ph} = 145e^{j2.33°}$ V

CHAPTER 5: CYLINDRICAL SHAPE DOUBLE-ROTOR PM MOTOR: OPTIMIZATION OF CORE DIMENSIONS AND DETERMINATION OF ELECTRO-MECHANICAL PARAMETERS

This chapter focuses on the design specifications for the cylindrical shape twin rotor PM motor and a working model is obtained in FEMM to optimize the motor core dimensions like rotor and stator core thickness. The results are further used to calculate the winding resistances and inductances and to plot the electromechanical characteristics of the motor like torque, emf and terminal voltage, for a given supply current.

5.1 Design Data of the Motor

A new concept of twin rotor cylindrical motor with slotless stator is introduced in this thesis. Each rotor carries sixteen magnetic pole pieces with three phase winding on the stator. The motor has been designed initially using the simplified magnetic circuit model. The motor dimensions determined this way are shown in Figure 5.1.

The aim of this project is to verify and optimize some of the motor elements like thickness of stator and rotor cores. The dimensions shown in Figure 5.1 (a) and Figure 5.1 (b) are used to construct the motor model in FEMM 4.0 software package.

The rotor core is made of solid steel and the stator core is laminated. To optimize the stator and rotor cores, it was assumed that the magnetic flux density in rotor should be around 1.5 Tesla and that in stator core to be 1.8 Tesla. The same material is used for the construction of rotor and stator cores of the cylindrical motor as the ones used for disc motor. Refer to Figure 4.2 in the previous chapter for the magnetization properties of the rotor and stator core materials.

The design specifications of the cylindrical shape double-rotor PM motor under consideration are stated in Table 5.1.
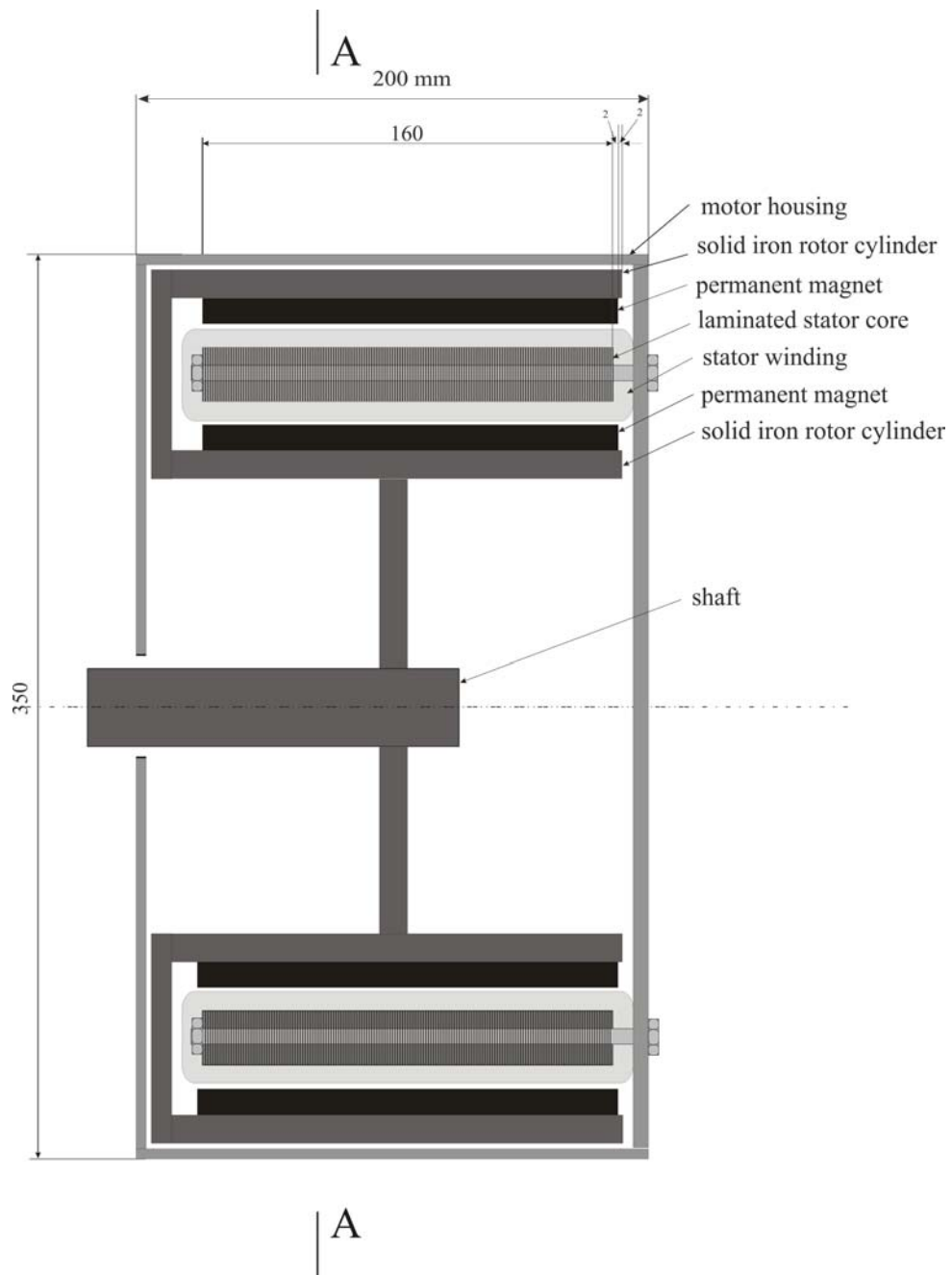
Figure 5.1(a): Scheme of the cylindrical shape double-rotor PMM with the dimensions marked
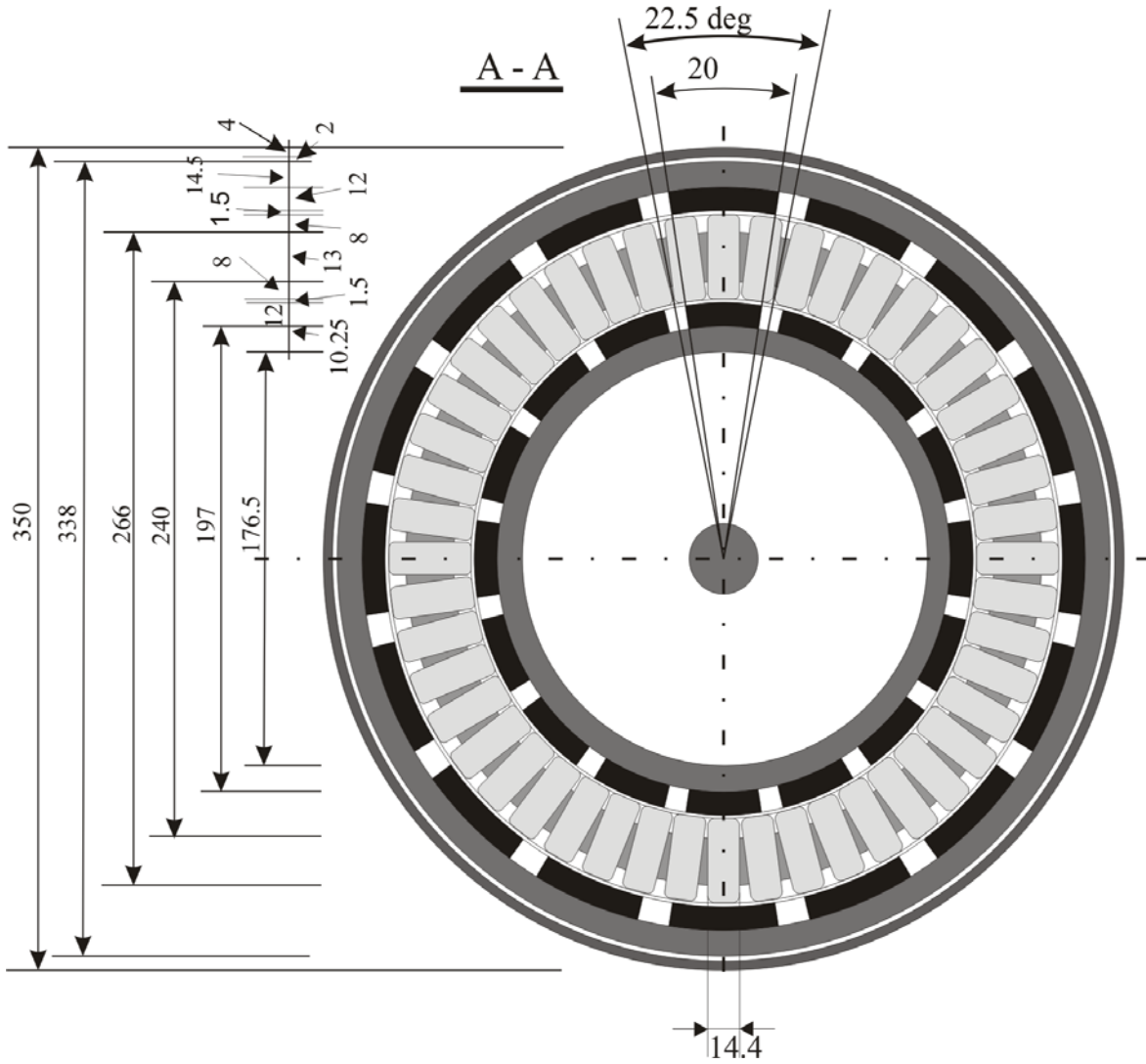
Figure 5.1(b): Perpendicular cross-section of the RFTR PM motor

Table 5.1: Design criteria for cylindrical shape double-rotor PM motor

Assumed data	
Magnetic pole number	16
Winding:	
- Number of phases	3
- Number of coils/phase/pole	1

(Table continued)

- Coil number	48
- Turn number/coil	10
- Wire diameter D_w	AWG9 – D_w=2.90575 mm,
- Coil cross-section area A_c=14.4x8	112 mm^2
- Wire cross-section area A_w	6.63 mm^2
- $k_{Cu} = \dfrac{A_w \times N_w}{A_C} = \dfrac{6.63 \times 10}{112} = 0.592$	
Rotor speed	822 rpm (86.08 rad/s)
Permanent magnet: $H_C = 979kA/m,$ $\mu_r = 1.049,$ $B_r = \mu_r H_C \mu_o = 1.2905T$	
Magnet thickness	12 mm
Flux density in the rotor discs (permissible)	1.5 T
Flux density in the stator discs (permissible)	1.8 T
Rotor core	Steel 1117
Stator laminated core	US Steel type 2-S, 0.018 inch thickness

The motor elements and electromechanical parameters of the cylindrical double-rotor PM motor that are to be determined are:

- **Design parameters to determine**

    - Thickness of the stator core (laminated steel)

    - Thickness of the rotor discs (solid iron)

- **Electromechanical parameters to determine**

    - Electromagnetic torque

    - Electromotive force

    - Phase Resistance

    - Self inductance

    - Mutual inductance

    - Voltage across terminals

5.2 Motor Model and Simulation in FEMM 4.0

Similar to the disc motor, as FEMM 4.0 allows only the construction of a 2-D model, the cylindrical shape double-rotor PM motor model is developed.

While drawing the model, an arbitrary value is assigned to the stator core thickness and to the inner and outer rotors core thickness, as well. This thickness is later scaled so as to obtain the desired magnetic flux density values in the rotors and stator. Once this is achieved, the final model of the motor is arrived at and this final model is analyzed to perform the remaining calculations. The magnetic poles and stator coils are marked by calculating their coordinates on the X-Y plane according to the angle subtended by them at the motor shaft. In other words, the radius and the angle subtended are translated to the Cartesian coordinates to be able to construct the motor model. The material properties and block labels, along with the circuit currents are assigned to each of the blocks in the model. A part of the FEMM 4.0 model of the RFTR PM motor with slot-less stator is shown in Figure 5.2 (a). Figure 5.2 (b) shows the model mesh, which depicts the triangulation in FEMM. Unlike the FEMM model of the disc shape double-rotor PM motor, this model is created for the entire cylindrical motor with all the sixteen magnetic poles. Hence, the results obtained are final and there is no need of manipulating them

as is the case with disc shape double-rotor PM motor. The results obtained are discussed in the subsequent sections of this chapter.
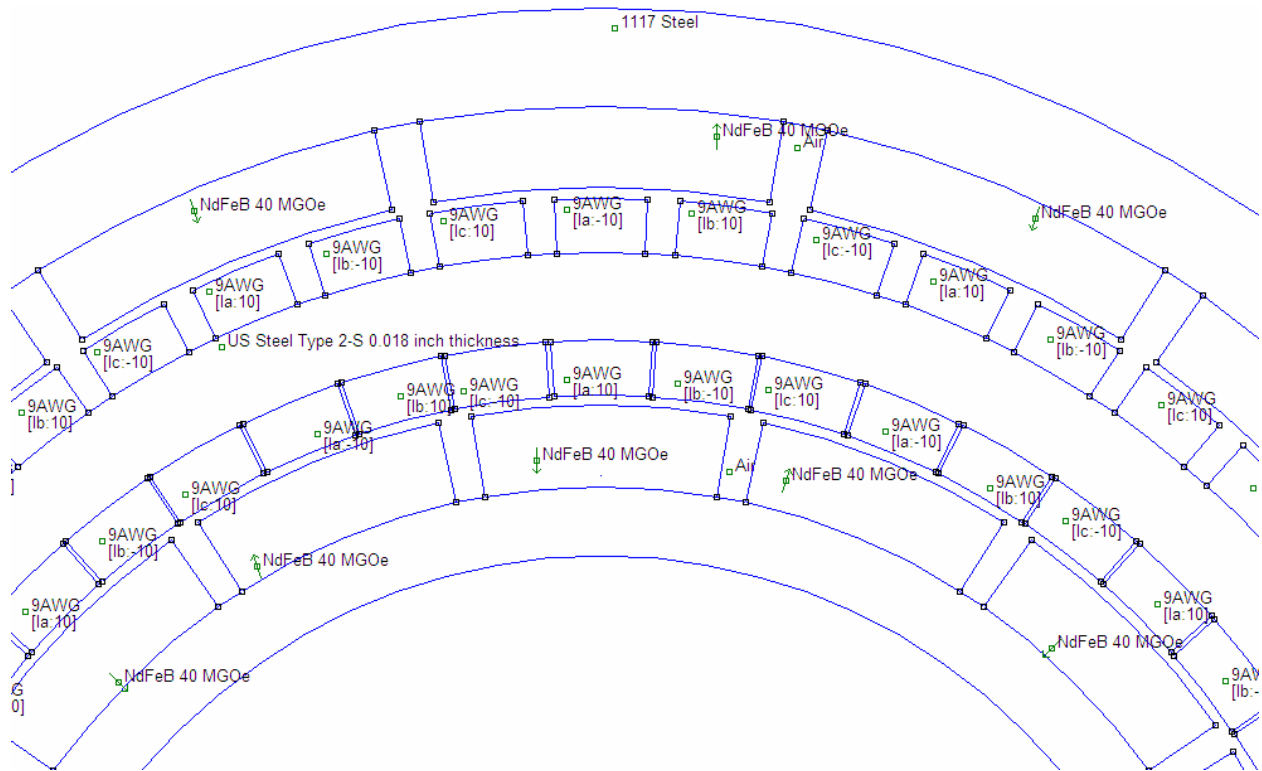
Figure 5.2 (a): FEMM 4.0 model for the RFTR PM motor

5.3 Magnetic Flux Distribution

In this subsection, the magnetic flux density distribution of the motor is determined and examined as to how the stator currents influence it. This study helps to analyze the torque developed by the motor. Figure 5.3 shows the current distribution in the stator coils. The magnetic field lines are generated by the permanent magnets and stator currents at a particular time instant. A more close up view of the current density distribution is shown in Figure 5.4, where the direction of the magnetic field is indicated by arrows and it can be observed that it is mainly a radial field in the air gap.
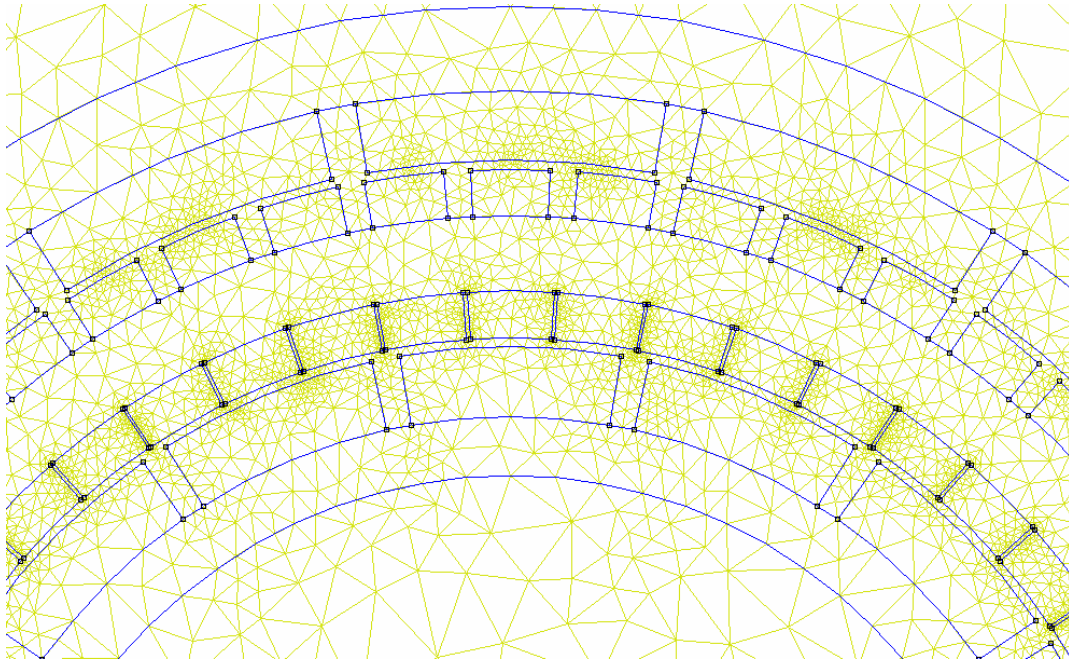
Figure 5.2 (b): Mesh of the FEMM 4.0 model of RFTR PM motor
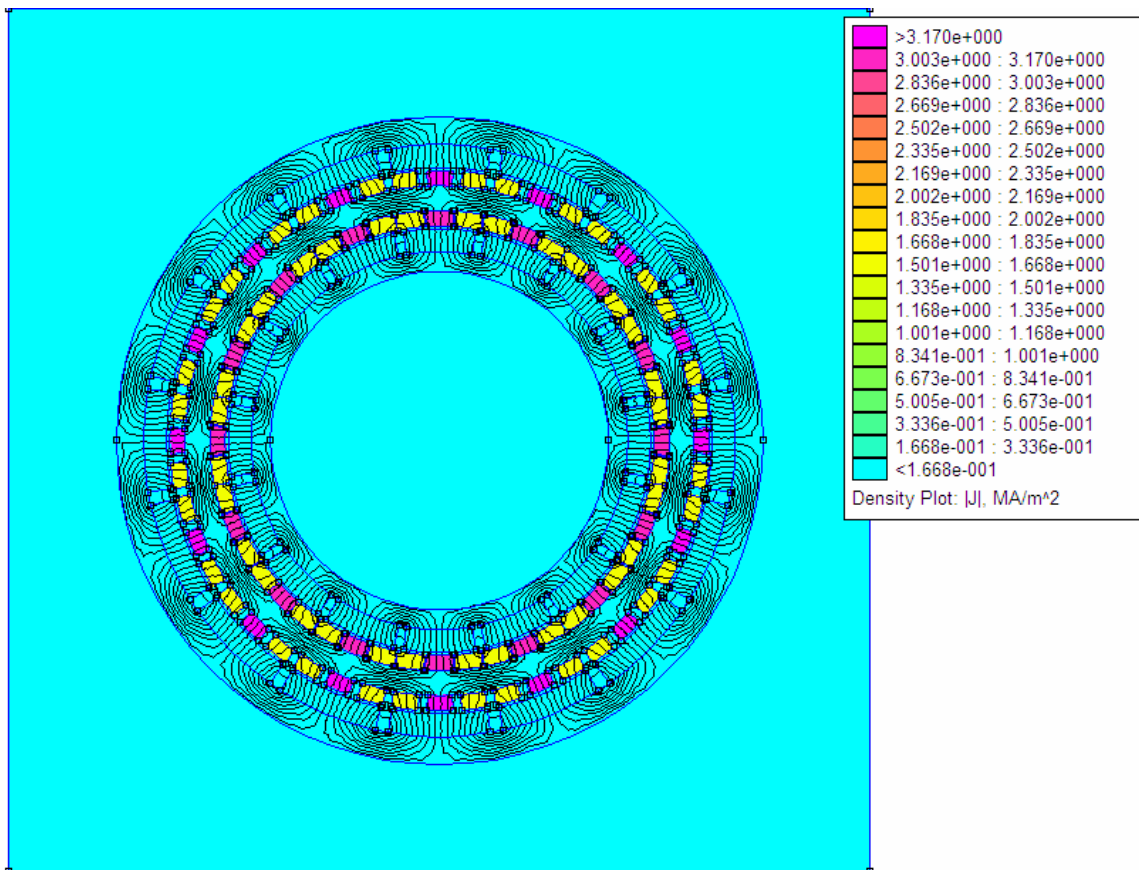
Figure 5.3: Current density distribution in the stator coils along with magnetic field lines
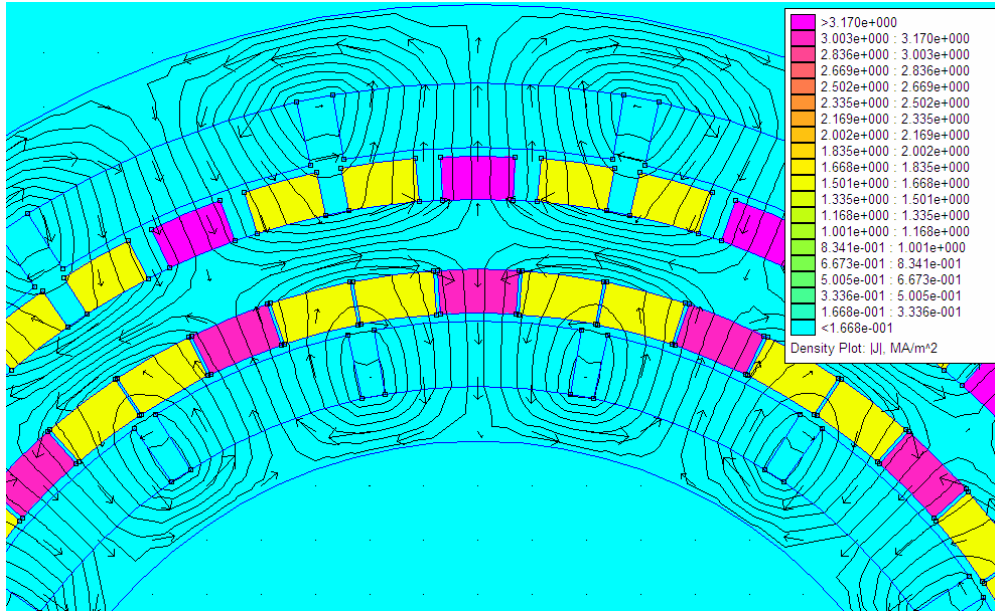
Figure 5.4: Direction of magnetic field in the motor

The magnetic flux density distribution in the motor, when the angle between rotor flux vector and current vector is 90°, is shown in Figure 5.5.

The stator core is made of laminated steel which goes into saturation at a higher flux density than solid iron, the material used for construction of rotor discs (Refer to Figure 4.2 in the previous chapter for the magnetization characteristics of the stator and rotor materials). Hence, one can observe that the flux density in stator core is higher than the flux density in rotor discs.

Figure 5.6 shows the magnetic flux density distribution for three different positions of the rotor with respect to stator.

The angle between the rotor flux vector and the current space vector is equal to 90°, 60° and 30° respectively for the following three plots. The presented results show negligible influence of magnetic flux generated by currents on PM flux.
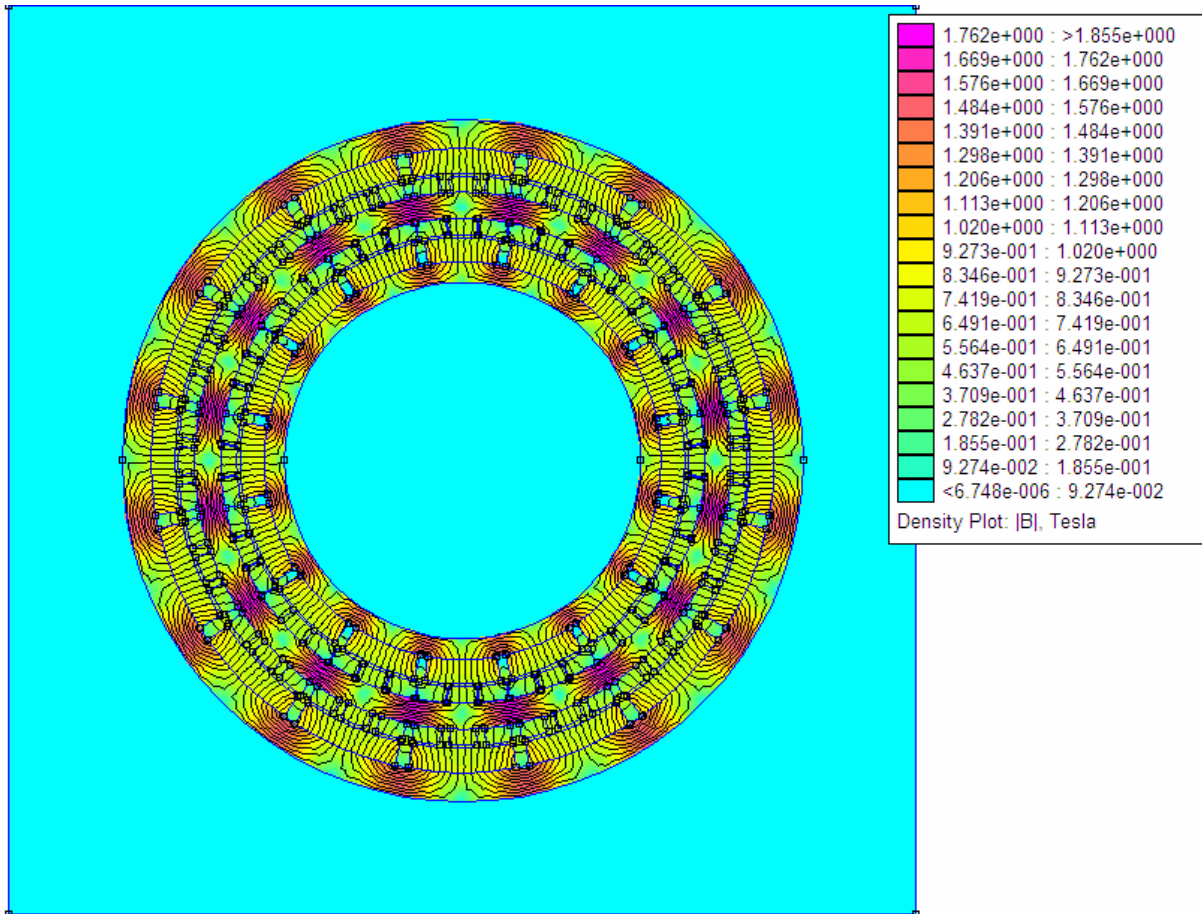
Figure 5.5: Flux density distribution for the cylindrical shape motor
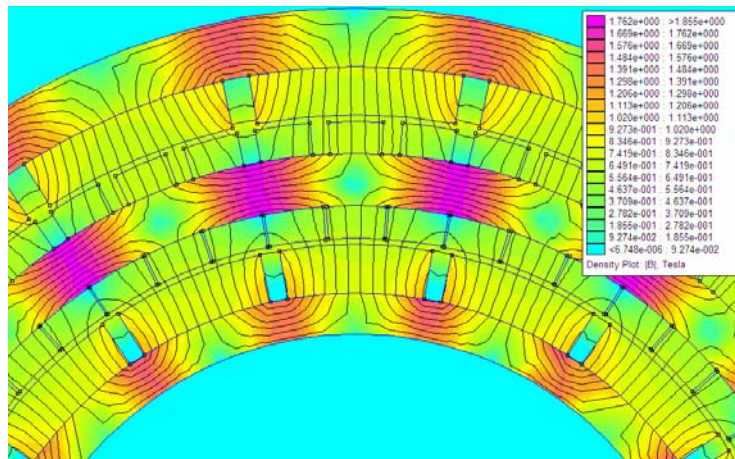
(a)

Figure 5.6: Flux density plots for the power angle of: (a) 90$^°$, (b) 60$^°$ and (c) 30$^°$ degrees

(Figure continued)
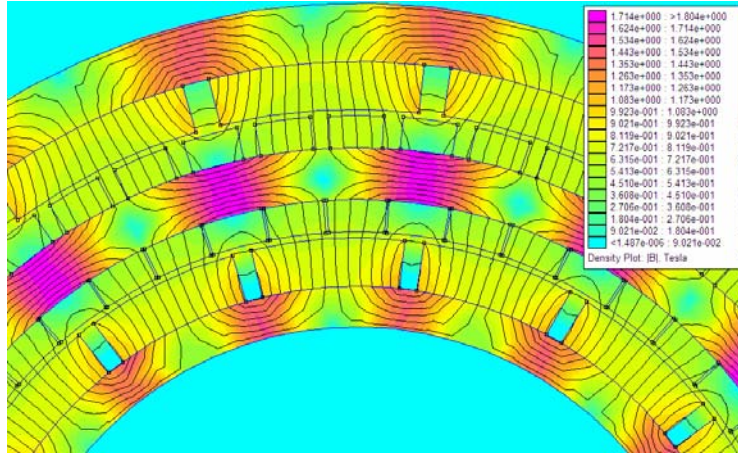
(b)
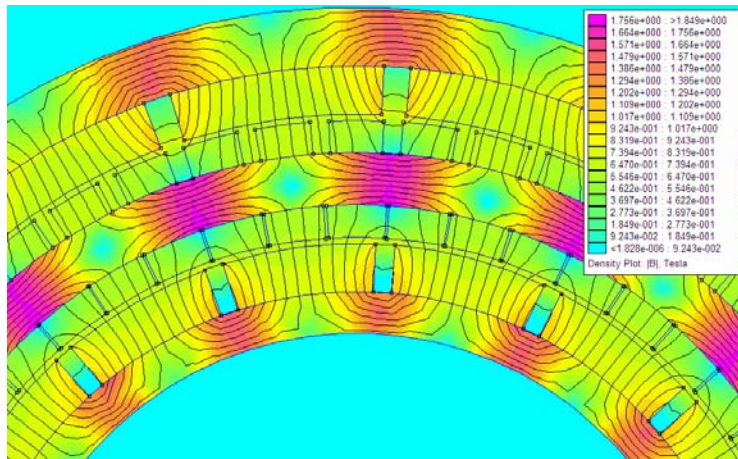
(c)

The normal component of magnetic flux density in the air gap between permanent magnet of the outer rotor and stator winding over the length of one pole pitch is determined and the plots are shown in Figure 5.7.

The three plots indicate the flux density distribution at power angles of 90°, 60° and 30° between the rotor flux and current space vector. No significant differences in flux density distribution are visible. It means that the stator current magnetic reaction on PM magnetic field is negligible.
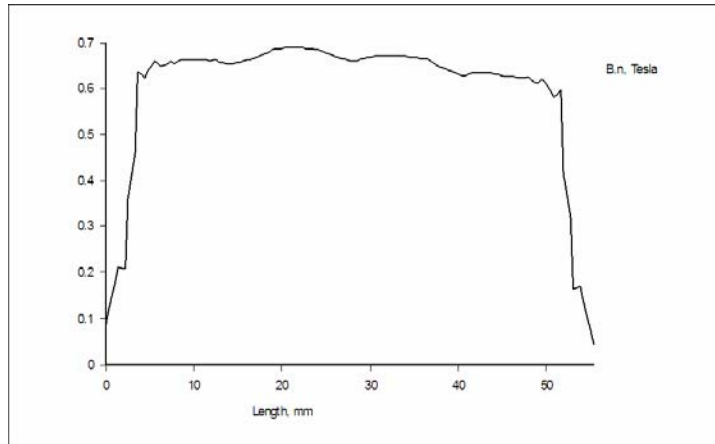
(a)
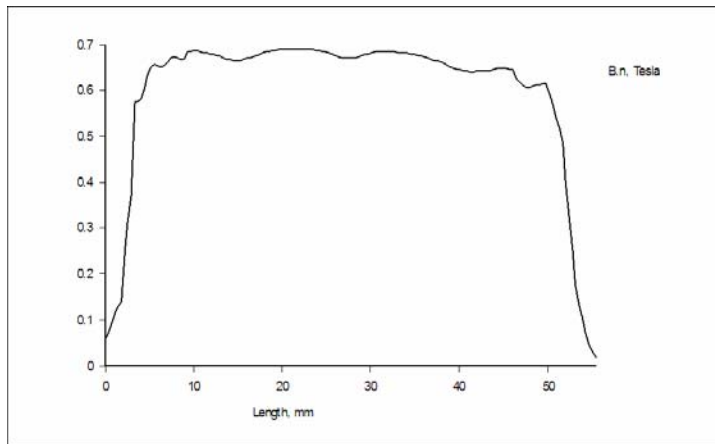
(b)
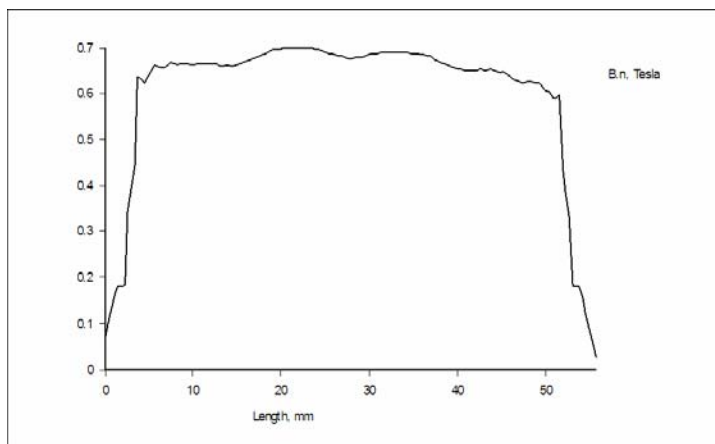
(c)

Figure 5.7: Magnetic flux density distribution in the air gap for power angle of: (a) 90°, (b) 60° and (c) 30°

5.4 Determination of Motor Parameters

5.4.1 Stator and Rotor Thickness

Keeping in mind the permissible magnetic flux density values to be achieved in the rotor discs and the stator core, the dimensions of each of these is adjusted in the FEMM motor model until the required values are obtained and the thickness of outer rotor is found to be 14.5 mm, inner rotor as 10.25 mm and that of the stator to be 13 mm. This way, it is made sure that the rotor flux density is around 1.5 T and the stator flux density is about 1.8 T.

5.4.2 Stator Winding Parameters

- **Phase resistance**

The phase resistance of the stator winding coil is calculated with the help of the following relation:

$$R = L_{c,av} \times N_W \times N_C \times R_{awg} \tag{5.1}$$

where L_{av} is the average length of the coil

N_W is the number of turns per coil

N_C is the number of coils per phase

R_{awg} is the resistance per kilometer of the AWG wire [11]

For the values of $L_{c,av}$ = 371.133 mm, N_W = 10, N_C = 16 and R_{awg} = 2.598 Ω, the phasor resistance of the stator coil winding is found to be 0.1543 Ω.

- **Self inductance**

The self inductance of each phase of the stator winding of cylindrical motor is calculated in a similar way as for the disc motor. The permanent magnets of the FEMM model are turned into air and current is assigned only to the phase whose self inductance is to be found. The

FEMM model is analyzed with zero currents in the other phases and the flux/current value is noted down, which is the value of self inductance of the phase considered. Hence, self inductance L is given by:

$$L = \frac{flux}{current}$$

(5.2)

The self inductance values for each of the phases are obtained as follows:

Self inductance of phase A, L_A = 0.3747 mH

Self inductance of phase B, L_B = 0.3735 mH

Self inductance of phase C, L_C = 0.3737 mH

- **Mutual inductance**

Like the case of self inductance, the permanent magnets are turned to air for calculating mutual inductance. The mutual inductance between phase A and phase B is obtained by assigning current to phase A and retaining zero currents in phase B and phase C. The flux linkage value for phase B is found by analyzed the motor model. This value divided by the phase A current gives the mutual inductance, M_{AB}.

$$M_{AB} = \frac{flux\ linkage}{I_A}$$

(5.3)

The mutual inductance values obtained between any two phases are given below:

Mutual inductance between phase A and phase B, M_{AB} = 0.1381 mH

Mutual inductance between phase B and phase C, M_{BC} = 0.139 mH

Mutual inductance between phase C and phase A, M_{CA} = 0.1379 mH

- **Synchronous inductance**

Synchronous inductance is the sum of self inductance and half of the value of mutual inductance (see equation 4.4). The synchronous inductance is thus obtained as follows:

$$L_S = L_{av} + 0.5M_{av} = 0.443 \text{ mH}. \tag{5.4}$$

5.5 Electromagnetic Parameters of the Motor

5.5.1 Electromagnetic Torque

The torque of a motor is proportional to the magnetic flux density, B and stator current, i which are in turn the functions of the space angle, θ.

$$T_{em} = K_T B(\theta) \times i(\theta) \tag{5.5}$$

Hence, a study is done on how the torque varies with the change of rotor position with respect to stator while keeping the current constant. The values are noted down and then, the stator currents are changed and the calculation is repeated by noting down the torque values as the space angle is changed. Finally, the stator currents are changed simultaneously as a function of the rotor mechanical angle and the pattern of the torque values is observed. The three cases are discussed in this subsection.

1) A current of magnitude 35.5A is supplied to phase A and the currents in phase B and phase C are maintained at zero.

   In the case of disc motor, a flat model of the motor is designed in FEMM where the curvatures are replaced by equivalent linear values, and hence the torque values are noted down with the change of electrical angle between the rotor and stator from $\theta = 0°$ to $360°$ for every $10°$ increment in the electrical angle (section 4.5.1). For the cylindrical motor in discussion, the entire motor model is developed in FEMM where the curvatures and angles subtended by the rotor magnetic pieces and stator coils at the shaft are represented as the data indicates. Hence, the torque values are obtained with the change of rotor mechanical angle from $\theta = 0°$ to $45°$, for every $1.25°$ increment in the mechanical angle. The relation between the electrical angle θ_e and mechanical angle θ_m is given as follows:

66

$$\theta_m = \frac{\theta_e}{p/2} \tag{5.6}$$

where p/2 is the number of pole pairs of the motor.

Once the corresponding phase currents are assigned to the motor model, the model can be analyzed by changing the rotor angle and the torque values can be noted down directly from the FEMM analysis. The plot is shown in Figure 5.8. It can be observed that the change in values follows a nearly sinusoidal pattern. This can be attributed partly to the slot-less stator core.
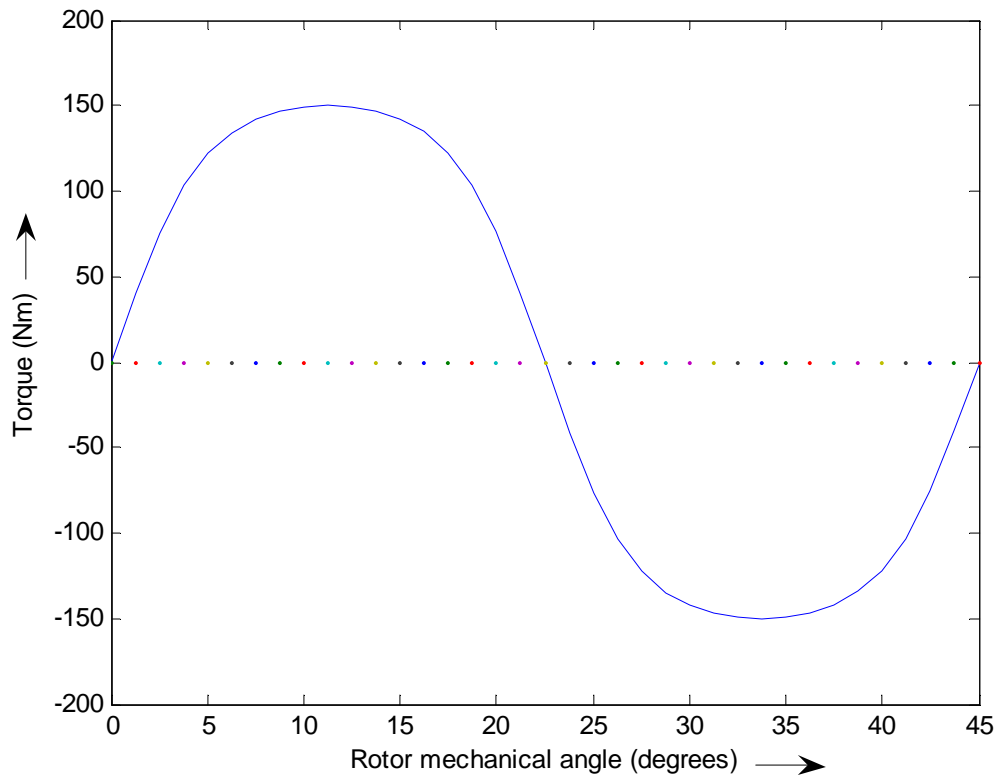
Figure 5.8: Electromagnetic torque developed by the rated current in phase A at different rotor positions

2) Phase A, B and C are supplied with DC currents of magnitude 35.5A, -17.75A and -17.75A respectively. The torque produced, by the resultant current vector and the rotor

magnetic flux, is noted down for various rotor angles. Figure 5.9 gives the corresponding plot. It can be noted that the change in torque is almost sinusoidal, which is the desired pattern as in the case of synchronous motors.
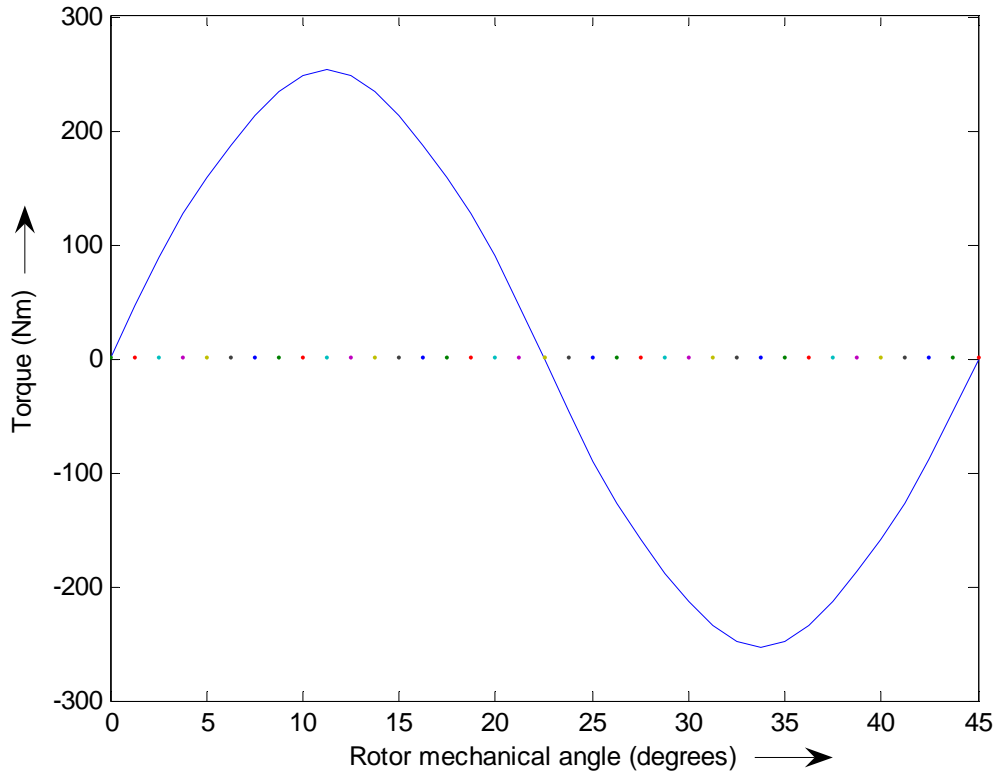
Figure 5.9: Electromagnetic torque developed by the motor at different rotor positions with respect to the stator current space vector

3) In this case, the phases A, B and C are supplied with the three phase sinusoidal currents according to the position of the rotor, that is, the rotor flux density vector (which is perpendicular to the current vector) and the current vector both move synchronously, as in the case of brushless DC motors. Thus, the torque changes with the position of both vectors, and has a range of $246Nm \leq T_{em} \leq 254Nm$, as indicated in Figure 5.10. The torque ripple is negligible, as a slot-less stator is used and no cogging torque is produced.

Please refer to Figure 4.12 in the previous chapter for the corresponding phasor and space vector diagrams.
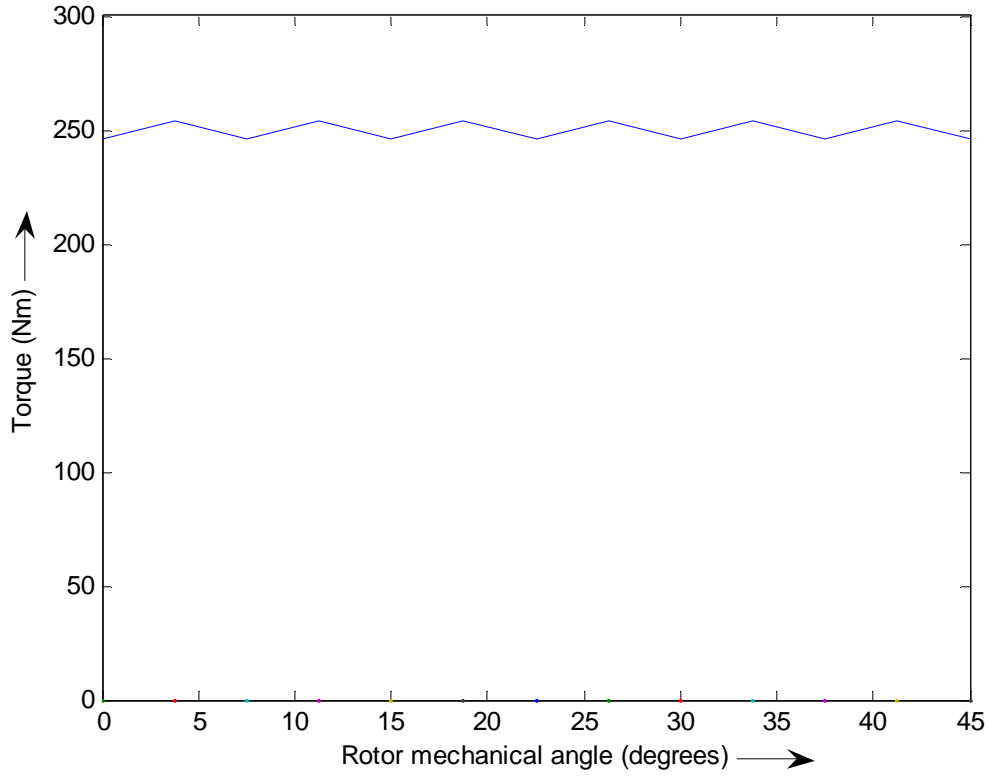
Figure 5.10: Electromagnetic torque vs. space angle θ determined at power angle of 90°

5.5.2 Electromotive Force

When the rotor rotates with respect to the stationary stator, an electromotive force is induced in the stator winding by the magnetic flux. Thus, the emf of any phase, which is a function of the rotor speed is given by the following equation:

$$e_{ph} = \omega_m K \tag{5.7}$$

where ω_m is the rotor speed in radians per second.

and $K = \dfrac{T_{em,ph}}{I_{ph}}$

To plot the emf as a function of the space angle, a DC current of 35.5A is supplied only to phase A of the motor model and the model is analyzed to obtain the values of torque at different rotor positions. These torque values are used to calculate the emf in phase A according to the equation stated above. The corresponding emf plot is shown in Fig 5.11.
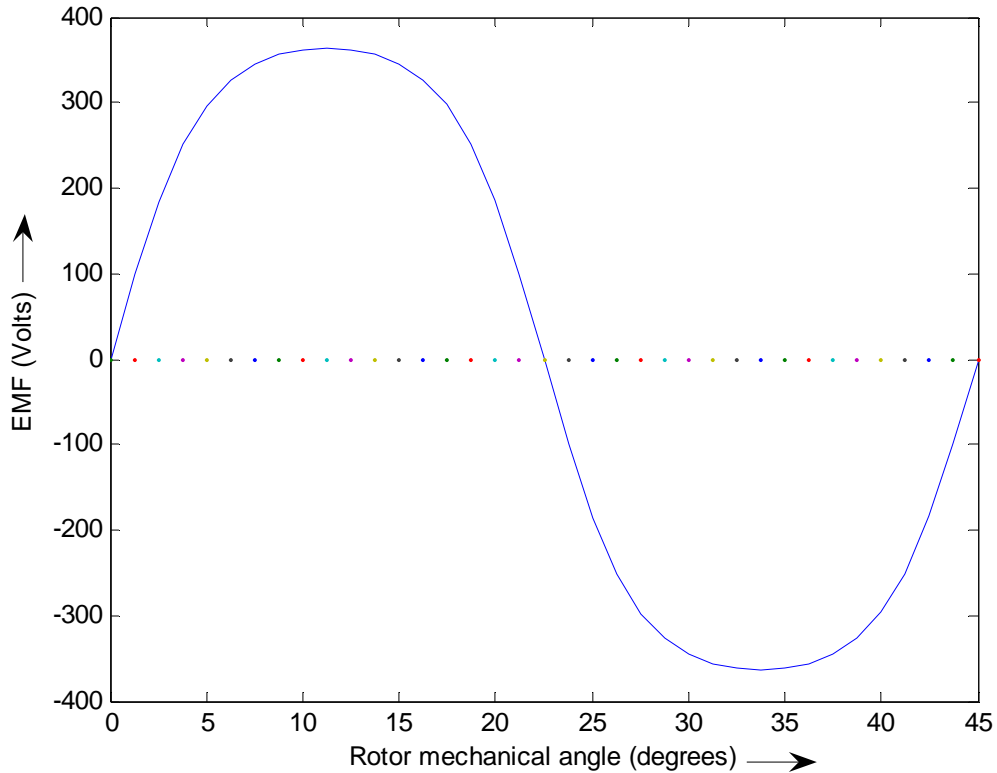
Figure 5.11: EMF induced plot as a function of space angle θ

5.5.3 Terminal Voltages

Similar to the theory stated for disc motor operating as a brushless DC motor, the voltage equation for the cylindrical shape double-rotor PM motor is given below (see Fig 4.15 for the equivalent circuit):

$$V_{ph} = E_{ph} + RI_a + jX_s I_a \tag{5.8}$$

where E_{ph} is the emf induced in phase A of stator winding

RI_a is the voltage drop across the resistance of phase A winding

jX_sI_a is the voltage drop across the phase A inductance

The voltage drops across the resistance and inductance are calculated with the help of design data provided and the results from FEMM analysis. These values are later added to the emf to obtain the total voltage drop across the terminals of the stator windings (see equation 4.9). For the values of R= 0.154 Ω and L_s= 0.443 mH, at the rated rotor speed of ω_m= 86.08 rad/sec,

$\omega_e = \dfrac{p}{2}\omega_m = 688.6rad/s$, $X_s = \omega_e L_s = 0.305\Omega$, emf E_{ph}= 257.61 V and for the AC current of

I_a= 35.5/$\sqrt{2}$ = 25.10 A, the voltage across the terminals, V_{ph} has a value of $262e^{j1.68°}$ V.

The phasor diagram corresponding to the above voltages is shown in Figure 5.12.
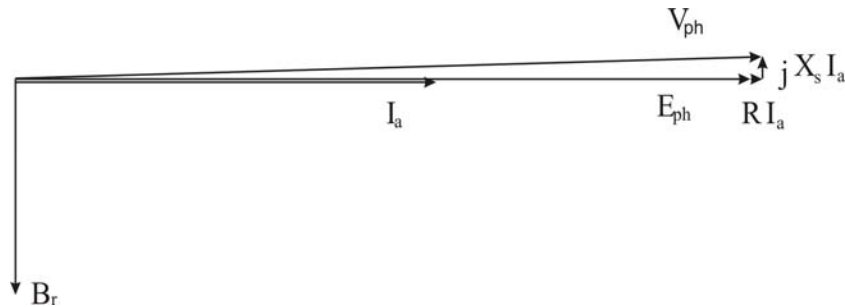
Figure 5.12: Phasor diagram for current and voltages of RFTR PM motor

CHAPTER 6: CONCLUSIONS AND FUTURE SCOPE OF STUDY

This chapter provides the conclusions to this thesis, offering a comparative study and analysis of the results obtained for the disc type double-rotor PM motor and the cylindrical shape double-rotor PM motor. A few of the possible avenues for further study on this topic are briefly discussed.

6.1 Comparison of Motors' Parameters

In the previous two chapters, the design parameters and the electromechanical parameters of both disc type and cylindrical shape double-rotor PM motors are calculated by developing FEMM models of the motors. The parameters which are most significant to the analyzed motors are given in Table 6.1.

Table 6.1: Parameters of disc type and cylindrical shape double-rotor PM motors

Motor parameters	Disc Motor	Cylindrical Motor
Supply voltage (V)	256	459
Current (A)	25	25
Speed (rpm)	822	822
Torque (Nm) (average value)	137	250
Mechanical power (KW)	12.00	21.50
Efficiency (%)	94.93	98.66
Motor volume (m^3)	0.0065	0.015
Motor mass (kg)	44.23	80.24
Torque/Volume (Nm/m^3)	21.06	16.23
Torque/Mass (Nm/kg)	3.10	3.11

Some of the parameters enclosed in Table 6.1 have been determined earlier. The others are calculated in the following way:

- Supply voltage (line to line voltage) of the three phase winding connected in Y is given by:

$$V = \sqrt{3} \times V_{ph} \qquad (6.1)$$

- Power (mechanical power on the motor shaft):

$$P = \omega_m T_{em} \qquad (6.2)$$

- Efficiency: The motor efficiency is calculated from the following equation:

$$Eff = \frac{P}{P_{in}} \times 100 \qquad (6.3)$$

where: P is the output power on the motor shaft

P_{in} is the input power given by $P_{in} = P + \Delta P_w$

ΔP_w is the power loss in the winding given by $\Delta P_w = 3 \times R_{ph} \times I^2$

- Motor volume: To calculate the motor volume, the outer dimensions and the active elements of the machine are taken into account as shown in Fig 6.1.

- Motor mass (mass of the active elements of the motor): To calculate the mass of the active elements of the motors, the following parts are considered.
  - For disc motor:
    - The two rotor rings of the double-rotor, whose dimensions are shown in Fig 6.2 (a): The volume of the rotor rings is $V_r = 122.52 \times 10^{-5}$ m³. With specific mass of steel, $\sigma_{Fe,r} = 7850$ kg/m³, the total mass of the rotor rings is given by:

$$M_r = V_r \times \sigma_{Fe,r} = 9.62 kg \qquad (6.4)$$
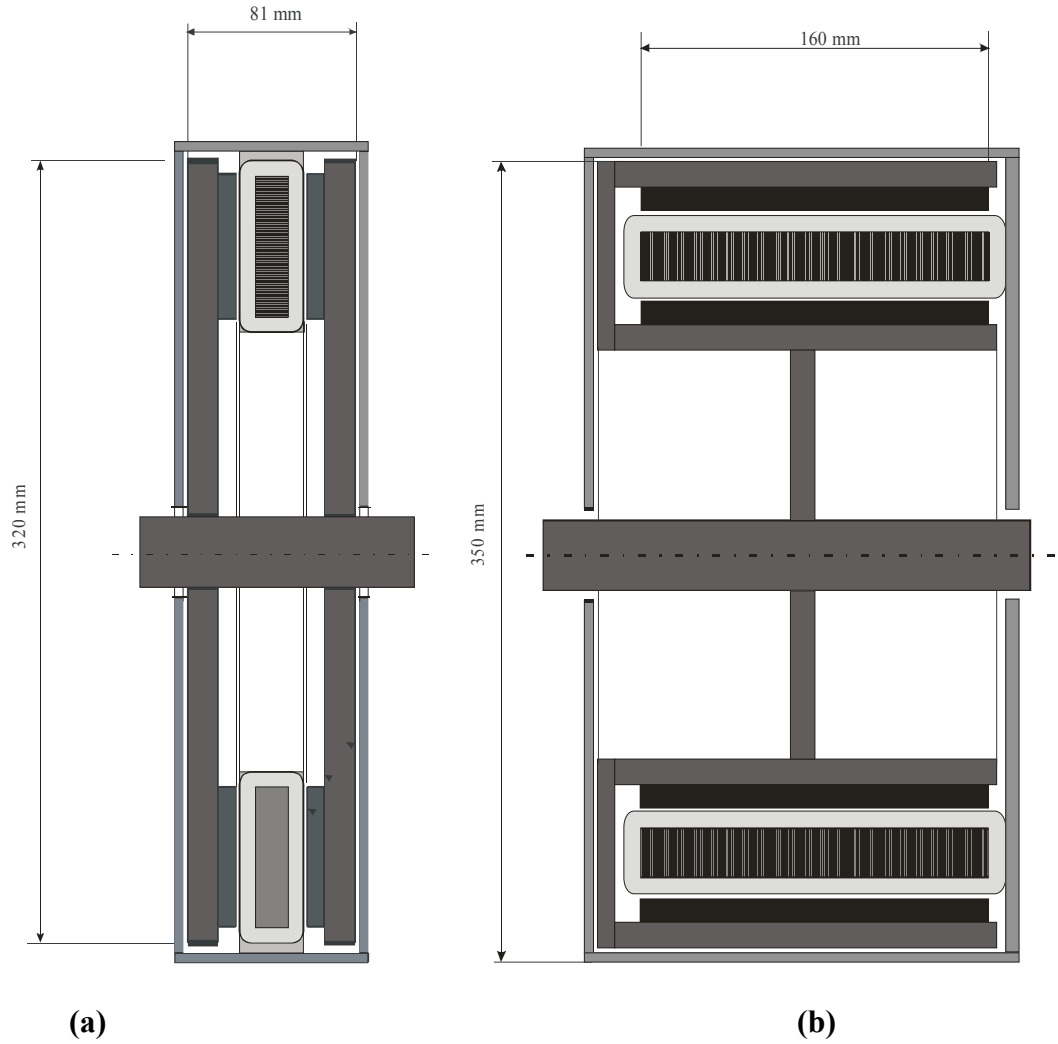
Figure 6.1: Main dimensions of: (a) disc motor, (b) cylindrical motor

- Magnets with dimensions shown in Fig 6.2 (b): The volume of a single magnet is obtained from FEMM as $V_{1m} = 8.64 \times 10^{-5}$ m^3. The total volume of all magnets is $V_m = 32 \times V_{1m} = 276.48 \times 10^{-5} m^3$. Since the specific mass of the magnetic material is σ_m =7650 kg/m^3, the total mass is obtained as:

$$M_m = V_m \times \sigma_m = 21.15 kg \qquad (6.5)$$
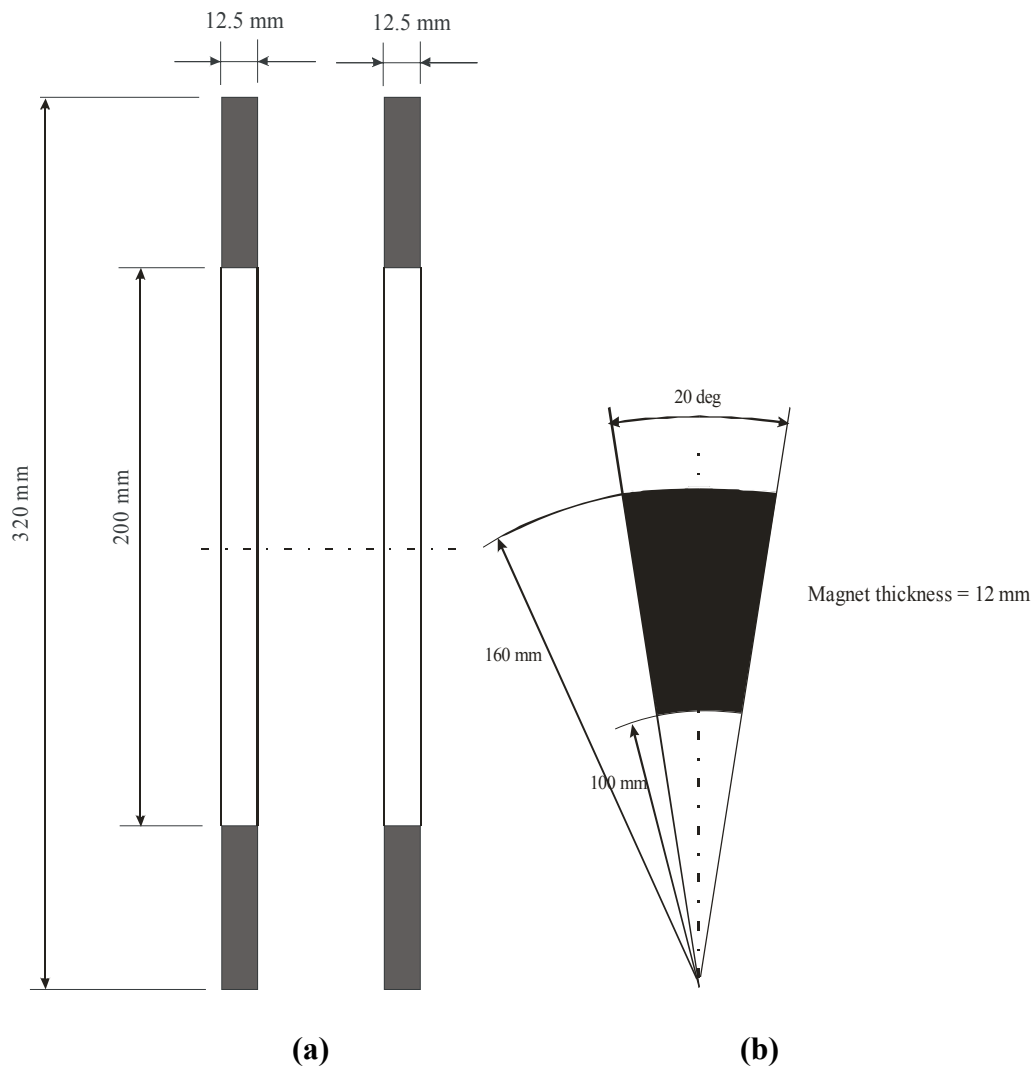
Figure 6.2: Dimensions of the active elements of disc motor: (a) rotor discs, (b) permanent magnet

- Stator ring, shown in Fig 6.2 (c): The volume of the stator ring is $V_s = 6.37 \times 10^{-4}$ m³. For specific mass of stator core, which is made of laminated steel, $\sigma_s = 7693$ kg/m³, the total mass of stator core is:

$$M_s = \sigma_s \times V_s \times K_s = 4.90 kg \qquad (6.6)$$

where: $K_s = 0.98$ which is a multiplicative factor for laminated steel.

13 mm

320 mm

200 mm

Figure 6.2. (c): Dimensions of stator core

- Copper winding: The wire used for the winding is AWG 11. Its diameter is 2.30×10^{-3} mm. The average coil length is calculated as $L_c = 171 \times 10^{-3}$ m. The total length of the wire per phase is $L_{ph} = N_c \times N_w \times L_c = 38.33$ m. The copper volume per phase is obtained as:

$$V_{Cu} = L_{ph}\left(\frac{d_w}{2}\right)^2 \times 2\pi = 319.58 \times 10^{-6}\, m^3 \qquad (6.7)$$

For the copper specific mass, $\sigma_{Cu} = 8930$ kg/m^3, the mass of wire per phase is:

$$M_{ph} = V_{Cu} \times \sigma_{Cu} = 2.85kg \qquad (6.8)$$

The total copper mass for the three phase motor is given by:

$$M_{Cu} = 3 \times M_{ph} = 8.56kg \qquad (6.9)$$

o For cylindrical motor:

- Two rotor cylinders (see Fig 6.3 (a)): The total volume of the cylinders is $V_r = 3.31 \times 10^{-3}$ m³. The total mass is calculated with the equation:

$$M_r = V_r \times \sigma_{Fe,r} = 26kg \qquad (6.10)$$

- Permanent magnets (Fig 6.3(b)): The volume of all the permanent magnets on the outer rotor is $V_{m,\,out} = 1.59 \times 10^{-3}$ m³ and the volume of PMs on the inner rotor is $V_{m,\,in} = 1.12 \times 10^{-3}$ m³. Hence, the total volume of PMs is 2.71×10^{-3} m³. The total mass of applied PMs is:

$$M_m = V_m \times \sigma_m = 20.72kg \qquad (6.11)$$

- Stator core (Fig 6.3 (c)): The volume of the stator core is $V_s = 1.65 \times 10^{-3}$ m³ and its mass is given by:

$$M_s = \sigma_s \times V_s \times K_s = 12.43kg \qquad (6.12)$$

- Copper winding: The wire used for winding is AWG 9, which has a diameter of $d_w = 2.91 \times 10^{-3}$ mm. The length of the wire per phase is $L_{ph} = 59.38$ m. The volume of copper per phase is $V_{Cu} = 0.79 \times 10^{-3}$ m³. The total mass of three phase winding is thus obtained as:

$$M_{Cu} = 3 \times V_{Cu} \times \sigma_{Cu} = 21.10kg \qquad (6.13)$$

(a)

20 deg

Magnet length = 160 mm

154.5 mm
142.5 mm
110.5 mm
98.5 mm
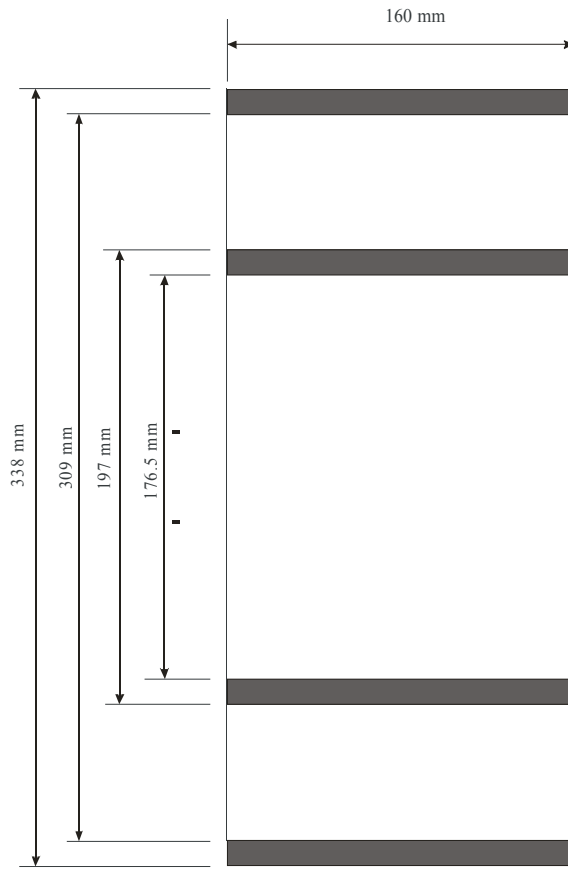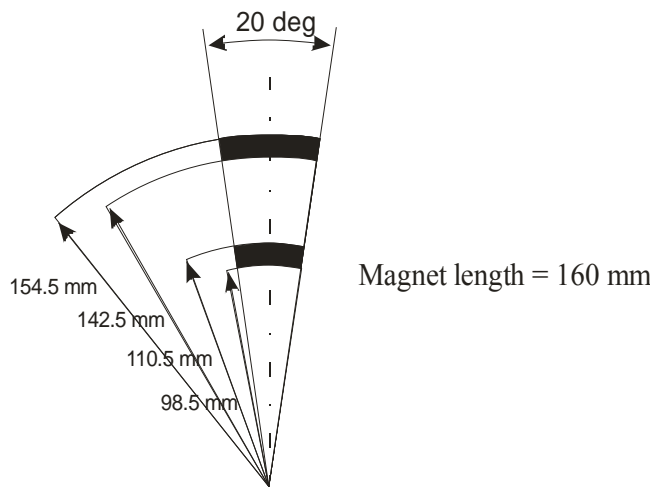
(b)

Figure 6.3: Dimensions of the active elements of cylindrical motor: (a) rotor cylinders, (b) permanent magnets, (c) stator core

(Figure continued)

78
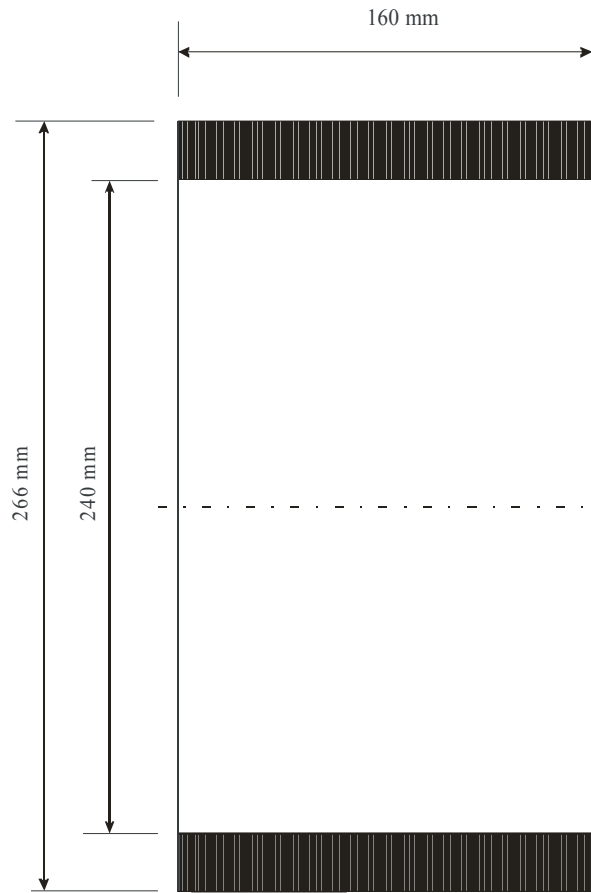
(c)

6.2 Conclusions

From the results obtained, the following conclusions can be arrived at.

- Both motors develop a torque which changes slightly in time at a constant supply current and constant speed (see Fig 4.13 and Fig 5.10). These changes however, are not significant. So, the motor can be applied to the drives where large torque ripple cannot be tolerated, for example, gearless drives for light electric vehicles or elevators.

- The efficiencies of both motors are high due to low power losses in the winding. These power losses are expected to be higher if the conventional winding with overlapping coils would be applied, which have much longer end connections.

These end connections do not contribute to the torque production but only to the copper power losses.

- However, it can be noticed that the efficiency of cylindrical motor is higher than that of disc motor. The relatively high efficiency of cylindrical motor may be contributed to low power losses because of shorter end connections of the windings than in the disc motor. It is anticipated that a multistage disc motor will have higher power losses due to more end connections and hence might not have higher efficiency than a cylindrical motor.

- Both the disc motor and cylindrical motor have almost equal torque/mass ratio. This means that they use almost same amount of material for their construction, for the production of torque. The torque to mass ratio is an important factor if the weight limit of the particular drive is crucial.

- The torque to volume ratio of the cylindrical motor is lower than that of the disc motor. It means that the disc motor is more compact and can be used in situations where the space limit is crucial (for example, elevator drive).

6.3 Future Scope of Study

The analysis carried out in this thesis is based on the motor magnetic field models developed in FEMM software package. It allowed to optimize the motor dimension and to determine the rated torque. The next stage, around which the future work should concentrate, is to analyze the performance of the motors in dynamic and steady-state conditions. This analysis should be done using the circuit models of the motors whose parameters (resistances and inductances) are determined in this research. To model the motor dynamics, the MATLAB/Simulink software package may be used.

BIBLIOGRAPHY

[1] Dr. Ernest Mendrela, "Introduction to brushless DC motors" Lecture notes, Louisiana State University, Baton Rouge, LA

[2] Harri Hakala, "Integration of Motor and Hoisting Machine Changes the Elevator Business" KONE Corporation Research Center, Finland.

[3] T. Kenjo and S. Nagamori, *Permanent-Magnet and Brushless DC Motors*, Clarendon Press, Oxford, 1985.

[4] Jacek F. Gieras and Mitchell Wing, *Permanent Magnet Motor Technology – Design and Applications, Second Edition, Revised and Expanded*, Marcel Dekker, Inc., New York, Basel.

[5] B.L. Theraja and A.K. Theraja, *A Textbook of Electrical Technology – In S.I. Units, Volume 2, AC & DC Machines*, S. Chand & Company Ltd., New Delhi.

[6] E. Mendrela, M. Łukaniszyn and K. Macek-Kamińska, *Disc-Type Brushless DC Motors*, Polish Academy of Science, 2002.

[7] Jacek F. Gieras, Rong-Jie Wang and Maarten J. Kamper, *Axial Flux Permanent Magnet Brushless Machines*, Kluwer Academic Publishers, The Netherlands, 2004.

[8] E. Mendrela, R. Beniak and R. Wrobel, "Influence of Stator Structure on Electromechanical Parameters of Torus-Type Brushless DC Motor" *PE-386EC*, 1999

[9] A. Afonin, P. Szymczak and P. Cierzniewski, "Disc-Motors with Permanent Magnets" XXXIII International Symposium on Electrical Machines, Permanent Magnet Electrical Machines, Poland, June 9-12, 1997.

[10] David Meeker, "Finite Element Method Magnetics – Version 4.0", User's Manual, January 8, 2006.

[11] Power stream: Wire gauge and current limits
http://www.powerstream.com/Wire_Size.htm

[12] Stephen J. Chapman, *Electric Machinery Fundamentals, Fourth Edition*, McGraw-Hill, 2005.

[13] A. Di Napoli, F. Caricchi, F. Crescimbini and G. Noia, "Design criteria of a low-speed axial-flux PM synchronous machine" University of Rome "La Sapienza" – Electrical Engineering Dept.

[14] F. Caricchi, F. Crescimbini, A. Di Napoli and E. Santini, "Optimum CAD – CAE design or axial flux permanent magnets motors" Universita' di Roma "La Sapienza".

[15] Professor O Honarati, Mr F Caricchi, Mr F Crescimbini, Professor A Di Napoli and Dr E Santini, "Axial-flux AC motor drives: A new solution for innovative electrical vehicles" Universita di Roma "La Sapienza".

[16] Han-Sam Cho and Hyun-Kyo Jung, Senior Member, IEEE "Analysis and Design of Synchronous Permanent-Magnet Planar Motors" IEEE transactions on energy conversion, Vol. 17, No. 4, December 2002.

[17] Deepti R Chikkam "Performance of disc brushless DC motor applied as gearless drive for wheelchair" Thesis document, Louisiana State University, Baton Rouge, December 2005

(a) M-file for plotting torque waveform in Fig 4.9

theta=[0, 10, 20, 30, 40, 50, 60, 70, 80, 90, 100, 110, 120, 130, 140, 150, 160, 170, 180, 190, 200, 210, 220, 230, 240, 250, 260, 270, 280, 290, 300, 310, 320, 330, 340, 350, 360];

torque=[0.036, 21.5168, 39.9743, 55.008, 65.5965, 72.5805, 77.2268, 80.1765, 81.7538, 82.2158, 81.8573, 80.391, 77.7053, 73.1415, 66.1943, 55.584, 40.2848, 21.453, 0.0623, -21.6173, -40.2923, -55.452, -66.1853, -73.0103, -77.6505, -80.4593, -81.8535, -82.2233, -81.7515, -80.1323, -77.3235, -72.645, -65.6003, -55.1348, -39.9878, -21.5708, 0.036];

plot(theta,torque,theta,0);

title('Torque plot for disc motor with no current in phases B and C');

xlabel('Rotor angle (degrees)');

ylabel('Torque (Nm)');

(b) M-file for plotting torque waveform in Fig 4.11

theta=[0, 10, 20, 30, 40, 50, 60, 70, 80, 90, 100, 110, 120, 130, 140, 150, 160, 170, 180, 190, 200, 210, 220, 230, 240, 250, 260, 270, 280, 290, 300, 310, 320, 330, 340, 350, 360];

torque=[0.0263, 24.684, 46.8278, 67.0418, 84.834, 100.6628, 115.6943, 128.328, 136.9358, 139.968, 137.1675, 128.901, 116.5058, 101.6168, 85.686, 67.7685, 47.3295, 24.741, -0.0458, -24.8783, -47.2935, -67.701, -85.674, -101.4203, -116.4795, -129.0105, -137.2208, -140.0093, -136.8368, -128.3198, -115.7445, -100.8345, -84.8265, -67.0935, -46.8945, -24.7448, 0.0263];

plot(theta,torque,theta,0);

xlabel('rotor angle (in degrees)');

ylabel('Torque (in Nm)');

title('Torque vs rotor angle with Ia=35.5A, Ib=Ic=-17.75A');

(c) M-file for plotting torque waveform in Fig 4.13

theta=[0, 30, 60, 90, 120, 150, 180, 210, 240, 270, 300, 330, 360];

torque=[134.5106, 139.9064, 134.5106, 139.9064, 134.5106, 139.9064, 134.5106, 139.9064,

134.5106, 139.9064, 134.5106, 139.9064, 134.5106];

plot(theta,torque,theta,0);

title('Torque plot with change of rotor angle and phase currents');

xlabel('Rotor angle (degrees)');

ylabel('Torque (Nm)');

(d) M-file for plotting emf waveform in Fig 4.14

theta=[0, 10, 20, 30, 40, 50, 60, 70, 80, 90, 100, 110, 120, 130, 140, 150, 160, 170, 180, 190,

200, 210, 220, 230, 240, 250, 260, 270, 280, 290, 300, 310, 320, 330, 340, 350, 360];

emf=[0.0873, 52.1739, 96.9297, 133.3834, 159.0584, 175.9932, 187.2596, 194.412, 198.2366,

199.3569, 198.4876, 194.9321, 188.4198, 177.3535, 160.5079, 134.7801, 97.6826, 52.0192,

0.1511, -52.4176, -97.7008, -134.46, -160.4861, -177.0354, -188.2869, -195.0977, -198.4784, -

199.3751, -198.231, -194.3048, -187.494, -176.1496, -159.0676, -133.6909, -96.9624, -52.3049,

0.0873];

plot(theta,emf,theta,0);

title('EMF plot for phase A of Disc Motor');

xlabel('Rotor angle (degrees)');

ylabel('EMF (Volts)');

APPENDIX B: M-FILES FOR CYLINDRICAL SHAPE DOUBLE-ROTOR PM MOTOR

(a) M-file for plotting torque waveform in Fig 5.8

theta=[0, 1.25, 2.5, 3.75, 5, 6.25, 7.5, 8.75, 10, 11.25, 12.5, 13.75, 15, 16.25, 17.5, 18.75, 20, 21.25, 22.5, 23.75, 25, 26.25, 27.5, 28.75, 30, 31.25, 32.5, 33.75, 35, 36.25, 37.5, 38.75, 40, 41.25, 42.5, 43.75, 45];

torque=[0.05936, 40.668, 75.8975, 103.367, 122.331, 134.412, 142.152, 146.879, 149.398, 150.225, 149.465, 146.909, 142.362, 134.704, 122.693, 103.754, 76.2918, 40.9079, -0.01186, -40.9593, -76.3191, -103.78, -122.704, -134.709, -142.352, -146.993, -149.443, -150.208, -149.406, -146.815, -142.121, -134.416, -122.323, -103.412, -75.9697, -40.6496, -0.008643];

plot(theta,torque,theta,0);

title('Cylindrical motor: Torque plot with single phase supply');

xlabel('rotor mechanical angle in degrees');

ylabel('torque in Nm');

(b) M-file for plotting torque waveform in Fig 5.9

theta=[0, 1.25, 2.5, 3.75, 5, 6.25, 7.5, 8.75, 10, 11.25, 12.5, 13.75, 15, 16.25, 17.5, 18.75, 20, 21.25, 22.5, 23.75, 25, 26.25, 27.5, 28.75, 30, 31.25, 32.5, 33.75, 35, 36.25, 37.5, 38.75, 40, 41.25, 42.5, 43.75, 45];

torque=[0.04815, 46.7849, 89.2284, 126.528, 158.796, 187.134, 212.966, 234.229, 248.283, 253.561, 248.529, 234.44, 213.369, 187.715, 159.361, 127.082, 89.7085, 47.0699, -0.01645, -47.1076, -89.7473, -127.091, -159.414, -187.752, -213.432, -234.529, -248.505, -253.493, -248.327, -234.139, -212.887, -187.171, -158.79, -126.55, -89.2948, -46.7647, -0.007787];

plot(theta,torque,theta,0);

title('Cylindrical motor: Torque plot with three phase supply');

xlabel('rotor mechanical angle in degrees');

ylabel('torque in Nm');

(c) M-file for plotting torque waveform in Fig 5.10

theta=[0, 3.75, 7.5, 11.25, 15, 18.75, 22.5, 26.25, 30, 33.75, 37.5, 41.25, 45];

torque=[246.166, 253.562, 246.166, 253.562, 246.166, 253.562, 246.166, 253.562, 246.166, 253.562, 246.166, 253.562, 246.166];

plot(theta,torque,theta,0);

xlabel('Rotor mechanical angle (degrees)');

ylabel('Torque (Nm)');

title('Torque of CM with change of rotor angle and change of stator currents simultaneously');

(d) M-file for plotting emf waveform in Fig 5.11

theta=[0, 1.25, 2.5, 3.75, 5, 6.25, 7.5, 8.75, 10, 11.25, 12.5, 13.75, 15, 16.25, 17.5, 18.75, 20, 21.25, 22.5, 23.75, 25, 26.25, 27.5, 28.75, 30, 31.25, 32.5, 33.75, 35, 36.25, 37.5, 38.75, 40, 41.25, 42.5, 43.75, 45];

emf=[-0.02096, 98.6118, 184.0363, 250.6443, 296.6282, 325.9222, 344.6902, 356.1522, 362.2603, 364.2656, 362.4227, 356.2249, 345.1994, 326.6303, 297.506, 251.5827, 184.9924, 99.1935, -0.0288, -99.3181, -185.0586, -251.6457, -297.5327, -326.6424, -345.1751, -356.4286, -362.3694, -364.2244, -362.2797, -355.997, -344.615, -325.9319, -296.6088, -250.7534, -184.2113, -98.5672, -0.02096];

plot(theta,emf,theta,0);

xlabel('Rotor mechanical angle (degrees)');

ylabel('EMF (Volts)');

title('EMF plot for phase A of Cylindrical motor');

VITA

Pavani Gottipati, daughter of Subhash Babu Gottipati and Ratnamala Gottipati, was born in Gudivada, India. She completed her schooling at Ramanath Secondary School, Visakhapatnam. She graduated in distinction from Andhra University with a degree of Bachelor of Technology in Instrumentation in 2004. She joined the Department of Electrical and Computer Engineering at Louisiana State University in August 2004 to pursue her master's. She will be awarded the degree of Master of Science in Electrical Engineering in August 2007.